Experimental Demonstration and Study of Transmembrane-Electrostatically Localized Protons Prevail

James Weifu Lee*

Department of Chemistry and Biochemistry, Old Dominion University, Norfolk, VA 23529 USA

ORCID: 0000-0003-2525-5870

*Corresponding Author email: jwlee@odu.edu

Abstract

In this review in relation to some interesting arguments from Silverstein, it is now reaffirmed that the experimental demonstration of transmembrane-electrostatically localized protons (TELPs) was successfully accomplished through 1) using an aluminum film as a TELPs sensor in a biomimetic anode water-membrane-water cathode system, 2) analyzing the water-electrolysis current curve, and 3) measuring bulk liquid phase pH. Formation of induced TELPs was subsequently discovered in an anode water-membrane-water-membrane-water cathode system. The discovery of induced TELPs enabled clean experimental tests on the cation-TELPs exchange process by using sodium bicarbonate or potassium bicarbonate solution in the central liquid chamber. The sodium/TELPs exchange equilibrium constant K_{pNa+} was determined to be (5.07 ± 0.97) x 10^{-8}. The potassium/TELPs exchange equilibrium constant K_{pK+} was determined to be (6.93 ± 1.23) x 10^{-8}. The analysis in this review affirmed that the experimental TELPs demonstration and the experimentally determined cation-TELPs exchange equilibrium constant values are valid. Silverstein's arguments appear to have stemmed largely from his own misunderstanding, such as his misconception on the aluminum film protonic sensing limit.

1. Introduction

Based on the fundamental understanding of liquid water as a protonic conductor, we have recently developed a transmembrane-electrostatically localized protons/cations charges (TELC) model (Lee, 2019a; 2020b; 2021b) that provides a unified framework to elucidate protonic cell energetics, including many experimental observations and explain bioenergetic systems, including both delocalized and localized protonic coupling (Lee, 2020a; Lee, 2020c; Lee, 2023b). The term TELC refers to the total transmembrane-electrostatically localized positive charges population that comprises the charges of both the transmembrane-electrostatically localized protons (TELP) and the associated transmembrane-electrostatically localized non-proton cations after the proton-cation exchanging process reaching equilibrium. TELC are instantly relevant to transmembrane potential, which we now understand is a function of TELC as in a TELC-membrane-anions capacitor (Lee, 2019a; Lee, 2020c). The formation of TELC-membrane-anions capacitors has been experimentally demonstrated using a biomimetic anode water-Teflon® membrane-water cathode system (Saeed and Lee, 2015; Saeed and Lee, 2018) through two PhD thesis research projects (Saeed, 2016; Kharel, 2024).

The TELC model (Lee, 2019a; Lee, 2020b; Lee, 2021b), which represents a complementary development to Mitchell's chemiosmotic theory, is highly useful in elucidating real-world bioenergetic systems with both delocalized and localized protonic coupling. For example, it has been successfully applied in elucidating the decades-longstanding energetic conundrum (Guffanti and Krulwich, 1984; Krulwich et al., 1998; Krulwich et al., 2011) of ATP synthesis in alkalophilic bacteria (Lee, 2015; Lee, 2017a; Lee 2017b; Lee, 2018; Lee, 2019b; Lee, 2020a) and in bettering the understanding of energetics in mitochondria (Lee, 2020b; Lee, 2021b). Its application has recently led to the identifica-

tion of the TELP thermotropic function as the Type-B energetic process (Lee, 2022a; Lee, 2022b; Lee, 2023c; Lee, 2024b; Sheehan *et al*., 2023) which can isothermally utilize environmental heat energy to do useful work in helping drive the synthesis of ATP (Lee, 2021a; Lee 2021b). Notably, independent researchers have now started to recognize the value of the TELC theory (Guan, 2022; Heine *et al*., 2023; Iovine *et al*., 2021; Lee *et al*., 2024; Teixeira *et al*., 2024) and successfully applied it in an excellent elucidation of the experimental observations (Hariharan *et al*., 2024) in a cellular membrane ion transport protein complex (melibiose transporter MelB) that could not be explained by any other existing models and/or theories.

According to the TELC theory (Lee, 2019a; Lee, 2020b; Lee, 2023a; Lee 2023d), transmembrane potential *(Δψ)* is a function of TELC surface density, as shown in the following protonic membrane capacitor-based equation with a voltage unit (V in volts):

$$Transmembrane\ potential\ (\Delta\psi) = \frac{S \bullet (TELC) \bullet e}{C} \quad \text{(Equation 1)}$$

where $\frac{S}{C}$ is the inverse of specific membrane capacitance *(C)* per unit surface area *(S)*; *TELC* is the number of positive charges per unit membrane surface area, which is the sum of transmembrane-electrostatically localized protons (TELPs) and transmembrane-electrostatically localized non-proton cations after cation exchange with TELPs; and *e* is a proton (or cation) charge of 1.60 x 10^{-19} Coulomb.

Accordingly (Lee, 2019a; Lee 2020b; Lee, 2023a; Lee, 2023d), when a transmembrane proton pumping process that is an electrogenic (*i.e*., electrically non-compensated) charge transport across a membrane charges up the membrane capacitor, a transmembrane potential (Δψ) will form. The formation of transmembrane potential (Δψ) has resulted from a protonic capacitor formation with transmembrane-electrostatically localized protons (TELPs) on the positive (such as mitochondrial cristae) side and with transmembrane-electrostatically localized hydroxide anions (also known as hydroxyl ions or anions) on the negative (e.g., mitochondrial matrix) side of the membrane.

In this article, we will review the evidence for the experimental demonstrations of TELP formation and testing of cation-TELPs exchange in biomimetic water-membrane-water systems and discuss the experimental results in relation to the interesting arguments from Silverstein (Silverstein, 2023).

2. Experimental TELPs demonstration in a biomimetic anode water-membrane-water cathode system.

To experimentally demonstrate transmembrane-electrostatically localized protons (TELPs) in relation to the protonic capacitor behavior (Equation 1), the experiments (Saeed and Lee, 2015) employed a biomimetic anode water-membrane-water cathode system where excess protons and excess hydroxide anions were generated by utilizing an "open-circuit" water-electrolysis system and their distributions were evaluated using a proton-sensing aluminum film as shown in *Figure 1* and in conjunction with electrolysis current monitoring and bulk liquid phase pH measurements.

2.1. Experimental TELPs demonstration in a biomimetic anode water-membrane-water cathode system using an aluminum film as a TELPs sensor.

To demonstrate the formation of TELPs, as previously reported (Saeed and Lee, 2015; Saeed, 2016), an ElectroPrep electrolysis system (Cat no. 741196, purchased from Harvard Apparatus Inc.) was employed with proton-impermeable membrane including Teflon films in the experiments as illustrated in *Figures 1 and 2.* The ElectroPrep electrolysis system *(Figures 1 and 2)* comprised a cathode chamber, a small Teflon center chamber and an anode chamber. The small Teflon center chamber *(Figure 2)* was inserted tightly through the middle of the inter-chamber wall (septum) with O-ring fitting (and with silicon-seal when necessary) that separates the cathode water chamber and the anode water chamber as illustrated in *Figure 1.* To evaluate the protonic capacitor concept predicted by the TELPs model, a 25-µm thick aluminum membrane (Al) was sandwiched in between two pieces of impermeable 75-µm thick Teflon (Tf) membrane disks (all with a diameter of 2.35 cm), forming a Tf-Al-Tf membrane disk *(Figure 2b)*. Alternatively, as specifically noted, an Al-Tf-Al film assembly which was made by sandwiching a Teflon (Tf) disk with two disks of Al film was employed as a protonic sensing membrane disk.

In the experiments, as illustrated in *Figure 1*, excess protons and excess hydroxide anions were generated in two water bodies separated by a membrane (Tf-Al-Tf or Al-Tf-Al) through "open-circuit" water-electrolysis. When the protonic capacitor across the membrane was charged up by the excess protons generated in the anode chamber and excess hydroxide anions in the cathode chamber, the electric current of the water electrolysis process

would approach zero, which can be analogous to a respiratory membrane system such as mitochondria with a fully charged membrane potential at its respiratory "state 4" resting stage (Nicholls and Ferguson, 2013).

It is known that an aluminum surface can begin to be corroded by protons when the effective proton concentration is above 0.15 mM (equivalent to a pH value below about 3.8) (Pourbaix, 1974a; Pourbaix, 1974b). This property was therefore employed as a proton-sensing mechanism in combination with the bulk phase pH measurement to determine the distribution of excess protons in the water-membrane-water system (*Figures 1 and 2a*). Based on the Al protonic sensing property, we predicted that TELPs that are formed at the positive liquid-membrane interface (P_I) facing the anode water could be powerful enough to corrode Al films. This predicated feature was exactly demonstrated through experimental testing.

As illustrated in *Figures 1, 2a, and 2c*, a Teflon membrane (Tf) was sandwiched between two pieces of aluminum film (Al), forming a proton-sensing Al-Tf-Al membrane system that separates the two water bodies: the cathode water body on the left and the anode water body on the right. During a 10-hour experiment with 200V-driven water electrolysis, it was noticed, as expected, the formation of small gas bubbles at both the anode and cathode platinum electrodes. This observation is consistent with the well-known water electrolysis process in which water is electrolytically oxidized to molecular oxygen (gas) producing protons in the anode water compartment while
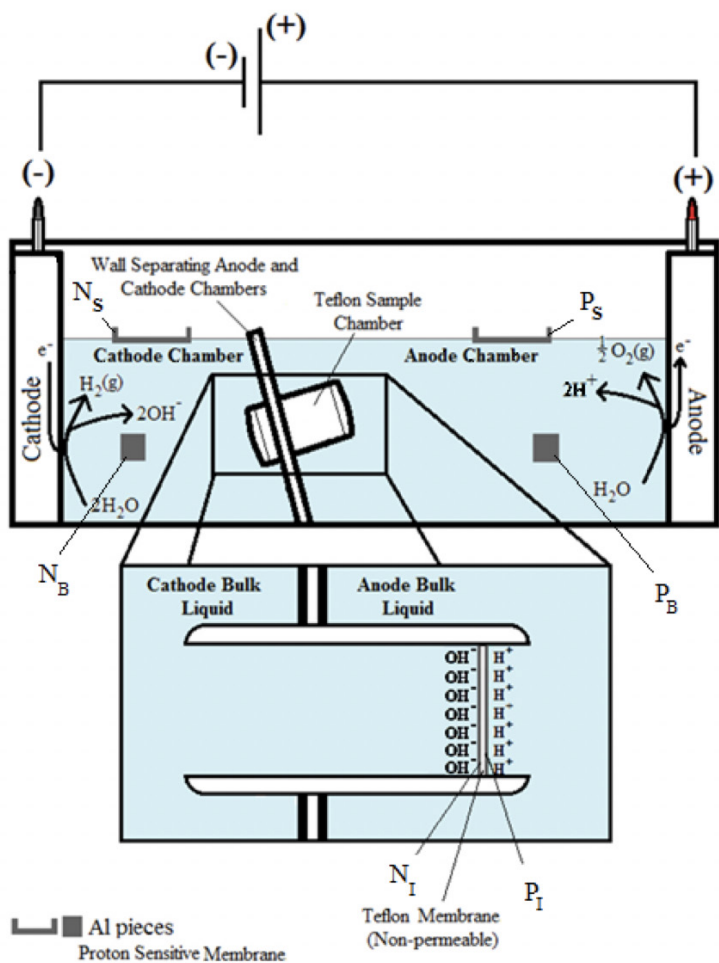

Figure 1. Illustration on how excess protons and excess hydroxide anions were generated by utilizing an ElectroPrep "open-circuit" water-electrolysis system comprising a cathode chamber, a Teflon center chamber assembly, and an anode chamber. The excess protons in the anode water were transmembrane-electrostatically localized at water-membrane interface (P_I) along the membrane surface while the excess hydroxide anions in the cathode water chamber (at the left) were attracted to the water-membrane interface (N_I) on the other side of membrane, forming a "hydroxide anions-membrane-excess protons" capacitor-like system (see Inset). Pieces of proton-sensitive Al films were applied on the anode water surface (P_S), the cathode water surface (N_S), in the middle of the anode chamber water bulk phase (P_B) and in the middle of the cathode chamber water bulk phase (N_B). Adapted from Ref (Saeed and Lee, 2015) and (Saeed, 2016).
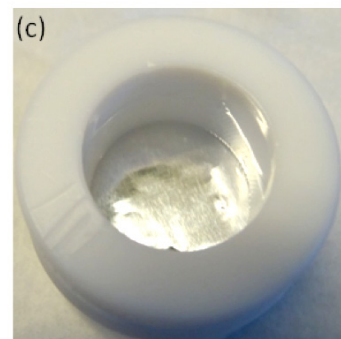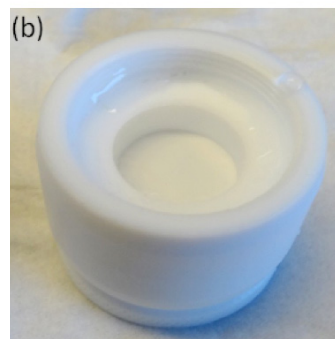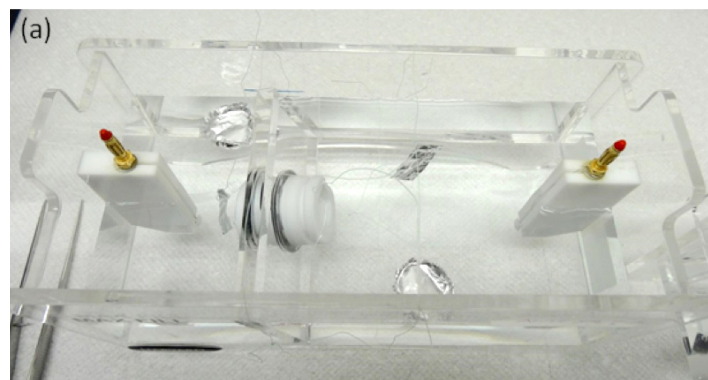

Figure 2. (a) A top view photograph showing the ElectroPrep apparatus. Pieces of proton-sensitive films were applied on the water surface and in the middle (bulk phase) of both the anode and cathode water chambers. Nylon strings were used to anchor the pieces of proton-sensitive films that were suspended in the middle of both the anode and cathode water chambers. **(b)** Teflon center chamber assembly with a Tf-Al-Tf membrane. **(c)** Teflon center chamber assembly with a proton-sensing Al-Tf-Al membrane.

protons are reduced to molecular hydrogen (gas) leaving more hydroxide anions in the cathode water compartment (Saeed, 2016).

The result of the "cathode water Al-Tf-Al water anode" experiment showed that only the proton-sensing film placed at the P_I site facing the anode liquid showed proton-associated Al corrosion (see the dark whitish grey gelatinous precipitate on the exposed portion of the proton-sensing film disk at P_I in *Figure 3*); on the other hand, the proton-sensing film placed in the bulk liquid phase (P_B) of the anode chamber or floated on the top surface (P_S) of the anode water body stayed pristine showing no proton-associated corrosion activity. This is a significant observation since it indicates that excess protons are transmembrane-electrostatically localized primarily along the water-membrane interface at the P_I site, but not in the bulk liquid phase (P_B). This observation agrees with the TELPs model prediction perfectly. Also as expected, all pieces of proton-sensing films placed at the N_I, N_B, and N_S sites of the cathode liquid showed no

proton-associated Al corrosion activity as well. These observations (*Figure 3*) all clearly confirmed the prediction from the TELPs model that <u>excess protons do not stay in the water bulk phase</u>; they are transmembrane-electrostatically localized at the water-membrane interface as part of the protonic capacitor behavior.

It is worth mentioning that the Al film in the Al-Tf-Al membrane does not serve as an electrode since the Al membrane itself was not connected to any external voltage source. It functioned as part of a protonic insulating membrane where excess protons accumulated at its surface on the P site while excess hydroxyl anions were localized at the N side as shown in *Figure 1*. When the effective proton concentration was above about 0.15 mM (equivalent to a pH value below 3.8) (Pourbaix, 1974a; Pourbaix, 1974b), the Al film proton-sensing detection employed here was in the form of protonic Al surface corrosion with the following major primary protonic Al corrosion reaction.
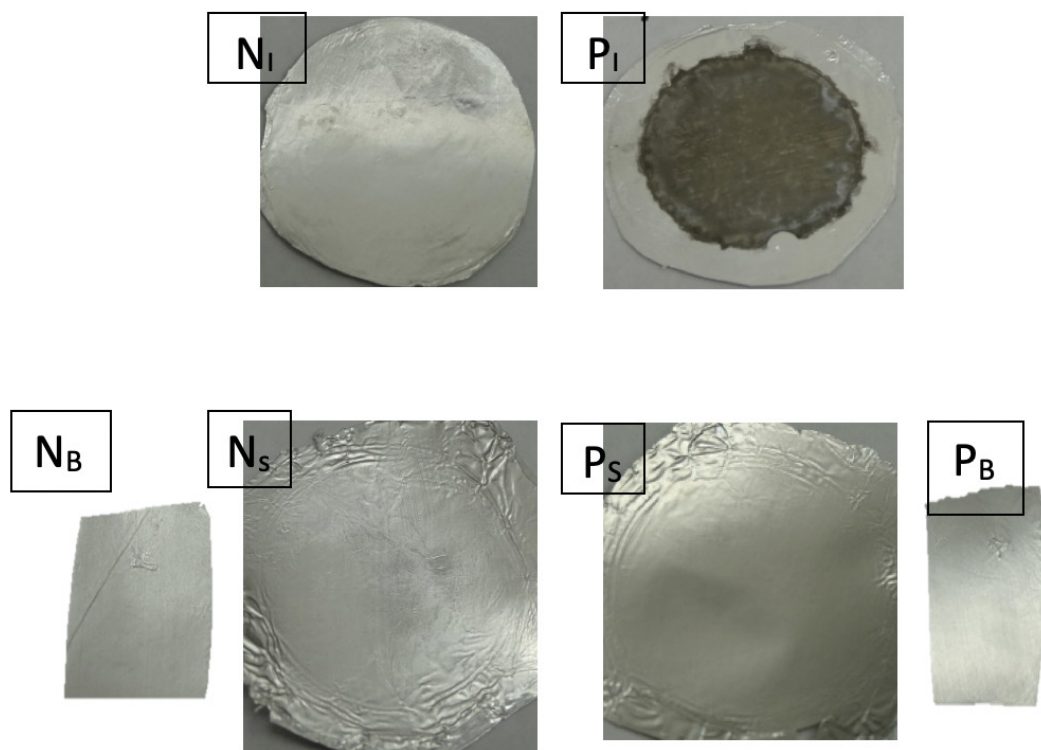
Figure 3: Observations with proton-sensing Al films after 10 hours of cathode water Al-Tf-Al water anode experiment with water electrolysis (200 V). N_I: Proton-sensing film at the N side of Teflon membrane detected no proton activity. P_I: Proton-sensing film at the P side of Teflon membrane detected dramatic Al corrosion activity of localized protons (dark whitish grey color). N_B: Proton-sensing film suspended inside the water of the cathode chamber. N_S: Proton-sensing film floating on the water surface of cathode chamber. P_S: Proton-sensing film floating on the water surface of anode chamber. P_B: Proton-sensing film suspended inside the water of the anode chamber. Adapted from Ref (Saeed and Lee, 2015) and (Saeed, 2016).

$$2Al(s) + 6H^+(TELPs) \rightarrow 2Al^{3+} + 3H_2(g) \qquad \text{(Equation 2)}$$

That is, the excess protons (TELPs) will oxidize metallic Al atoms, producing Al^{3+} ions and dihydrogen (H_2) gas as shown in Equation 2. Therefore, we predict that the TELPs Al corrosion process will produce gas (H_2) bubbles. This predicted feature was demonstrated exactly in the experiment, where we indeed noticed the formation of gas bubbles on the aluminum membrane surface at the P_I site as shown by the photograph in *Figure 4*.

Furthermore, the produced Al^{3+} cations can diffuse and interact with water and subsequently take hydroxide anions in the liquid to produce aluminum hydroxides [$Al(OH)_3$], which can form a gelatinous grayish/whitish milky precipitate in water. When the grayish/whitish precipitate builds up, the TELP Al film corrosion stain could look somewhat darker, whitish grey depending on the laboratory lighting conditions. This Al corrosion activity was exactly what we observed at the TELP site (P_I) in the experiment *(Figures 3 and 4)*.

As shown in *Figure 4,* many gas (H_2) bubbles were evolving from the P_I site of the Al-Tf-Al disk that was exposed to the anode chamber water at the right end of the central chamber channel. It was noticed that more gas (H_2) bubbles were evolving from the Al-Tf-Al disk rim (edge) than the central portion of the disk surface. The Al corrosion gelatinous product at the central portion of the disk looks whitish grey while the corrosion stain around the disk rim apparently resulted in a grayish dark ring. These observations indicated that the protonic corrosion activity around the disk rim (edge) appears to be somewhat stronger than that on its center part of the disk. That is, the gelatinous product precipitate color of TELPs-associated Al corrosion on an Al film could vary from light whitish grey to dark whitish grey, which may represent the differences in the degree (intensity) of TELPs-associated Al corrosion.

2.2. Experimental TELPs demonstration in a biomimetic anode water-Teflon membrane-water cathode system by analyzing the water-electrolysis current curve.

Furthermore, the experiments (Saeed and Lee, 2015) reproducibly demonstrated the formation of TELPs also by measuring the water electrolysis/protonic capacitor charging up curve as well. Teflon (Tf), which is impermeable to protons and has a dielectric constant of 2.1 like that of lipids, is a good insulating material to use to mimic the insulating property of a biomembrane to demonstrate TELPs formation. As shown in *Figure 1*, the proton-charging-up process in this "excess hydroxide anions Tf-Al-Tf excess protons" capacitor system was monitored by measuring the electric current of the 200V-driven water electrolysis process as a function of time during the entire 10-hour experimental run. The data in the inset of *Figure 5* showed that the electric current of the water electrolysis process decreased with time as expected. That is, when the excess protons were generated in the anode water compartment (while the excess hydroxide anions were generated in the cathode water compartment), this "excess hydroxide anions Tf-Al-Tf excess protons" capacitor is being charged up by transmembrane-electrostatic localization of the excess protons at the P_I site and the excess hydroxide anions at N_I site (*Figure 1*). According to the analysis, this process reached thermodynamic equilibrium after about 1500 seconds (shown in the inset of *Figure 5*) under this experimental condition where the curve of the water electrolysis current quickly became flat indicating the completion of the water electrolysis-coupled protonic capacitor-charging-up process.

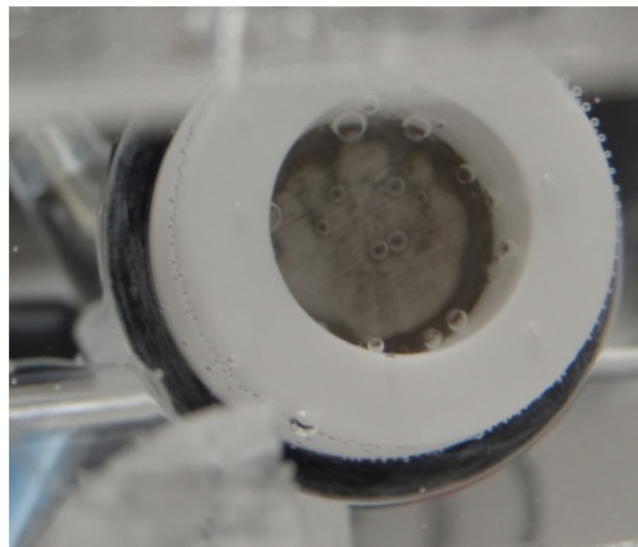As recently reported (Saeed and Lee, 2015; Saeed, 2016),

Figure 4. Teflon center chamber (with Al-Tf-Al membrane) after 10 hours electrolysis. Formation of gas bubbles and substantial TELP activity was noticed on the aluminum film surface at the P_I site. Note, the more or less dark whitish grey gelatinous precipitate that is covering the Al film disk at the P_I site. It appears to have more gas (H_2) bubbles evolving from the Al film disk edge (rim) where more protonic corrosion product is building up, showing more of a "more dark whitish grey gelatinous precipitate ring" in comparison with whitish grey gelatinous precipitate on the central portion of the disk in the Teflon chamber channel that faces the anode chamber water. Adapted from Ref (Saeed, 2016).

by calculating the area under the water-electrolysis protonic capacitor-charging-up current curve above the flat baseline as shown in the inset of *Figure 5*, the amount of excess protons loaded onto the entire "cathode chamber water Al-Tf-Al water chamber anode" experimental system (*Figure 1*) including the "excess hydroxide anions Tf-Al-Tf excess protons" capacitor and the septum that separates the cathode chamber water and the anode chamber water was estimated to be 2.98×10^{-13} moles.

As listed in *Table 1*, since the 25-μm Al film in between the two Tef films (each has a thickness of 75 μm) is a conductor, the Tf-Al-Tf membrane disk assembly had an effective insulating (Tf) membrane thickness of 75 + 75 = 150 μm. The Tf-Al-Tf membrane disk assembly was held at the right end of the Teflon center sample chamber that was tightly inserted into a septum also known as the "wall separating anode and cathode chambers" as illustrated in *Figure 1*. The area of the 150-μm thick Tf disk exposed to the anode water at the P_I site was measured to be 2.55 cm². The Septum was 0.8 cm thick, and its area exposed to the anode water was 51.2 cm² as calculated from its length of 9.6 cm and width of 5.6 cm.

Since the septum was in contact with the anode liquid at the positive side and the cathode liquid at the negative side (as shown in *Figure 1*), it could, to some extent, also behave like a protonic capacitor like the Tf-Al-Tf membrane. Therefore, we calculated the capacitance values for the 0.8 cm thick septum and the 150-μm thick Tf disk (Tf-Al-Tf membrane) from their thickness, dielectric constant (2.1) and the relevant surface area. As shown in *Table 1*, the capacitance values of the Tf-Al-Tf membrane disk and the septum were calculated to be 3.16×10^{-11} and 1.19×10^{-11} Farad, respectively. The ratio of the 150-μm thick Tf disk capacitance to the septum capacitance is 2.66/1. Based on this ratio, 72.6% of the excess protons (2.98×10^{-13} moles) are on the 150-μm thick Tf disk surface (2.16×10^{-13} moles). The TELP density of 8.49×10^{-14} moles/cm² on the 150-μm thick Tf disk is 53 times as high as that on the septum surface (1.59×10^{-15} moles/cm²). The thickness of the TELP layer is likely to be about 1 nm
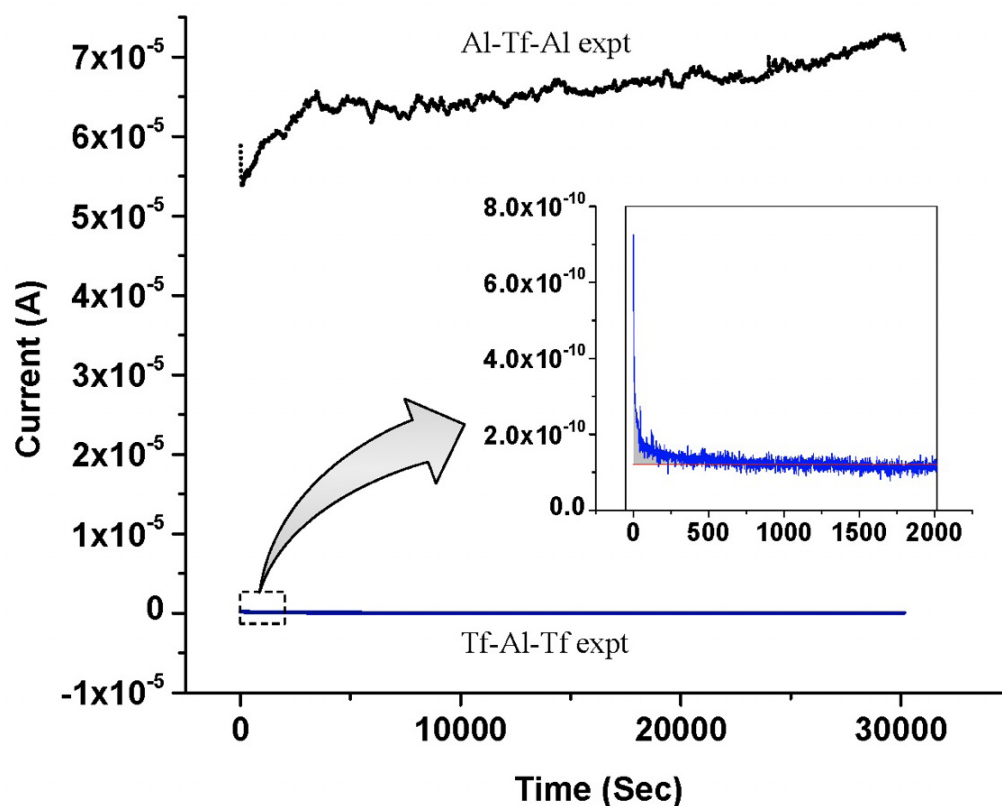
Figure 5. The electric current of water electrolysis measured as a function of time with 200 V for 10 hours experimental run. The black curve shows average of three experiments with "cathode water Al-Tf-Al water anode". The blue line shows average of three experiments with "cathode water Tf-Al-Tf water anode"; and its initial part within the first 2000 seconds is plotted in an expanded scale showing the integration for the area under the curve (Inset). Adapted from Ref (Saeed and Lee, 2015) and (Saeed, 2016).

but its exact thickness currently is still not entirely clear (Lee, 2015). Assuming the thickness of the TELP layer to be about 1 nm, the TELP concentration at the liquid-membrane interface along the positive side of the Tf-Al-Tf membrane was calculated to be 8.49×10^{-4} M, which is substantially higher than that (1.59×10^{-5} M) of the 0.8-cm thick septum.

The water electrolysis current in the "cathode water Al-Tf-Al water anode" experiment was also monitored. As shown in *Figure 5,* after about 5000 seconds, the water electrolysis electric current at the steady state of this experiment reached around 6.5×10^{-5} A, which was much bigger than that (below 1×10^{-10} A) of the "cathode water Tf-Al-Tf water anode" experiment. This large water electrolysis electric current can be attributed to the active consumption of excess protons by the proton-sensing Al film corrosion process at the P_I site. As the proton-sensing film corrosion at the P_I site consumes the excess protons, more excess protons can then be produced at the anode electrode, resulting in a high water-electrolysis electric current. The high concentration of TELP at the P_I site thermodynamically drives the aluminum corrosion reaction in which aluminum atoms are oxidized by excess protons resulting in evolution of molecular hydrogen gas as shown in Equation 2 and *Figure 4.*

2.3. Experimental TELPs demonstration in a biomimetic anode water-membrane-water cathode system by measuring bulk liquid phase pH.

The protonic capacitor feature (Saeed and Lee, 2015) that excess protons do not stay in the bulk water phase was reproducibly demonstrated also by the experimental observation that the measured pH value in the anode bulk water body remained essentially the same as that of the

	Area (cm^2)	Dielectric constant	Capacitance (Farad)	TELP (moles)	TELP density (moles/cm^2)	TELP molar concentration if l = 1 nm
0.8-cm thick septum	51.2	2.1	1.19×10^{-11}	8.15×10^{-14}	1.59×10^{-15}	1.59×10^{-5} M
150-μm thick Tf disk	2.55	2.1	3.16×10^{-11}	2.16×10^{-13}	8.49×10^{-14}	8.49×10^{-4} M

Table 1. The calculated capacitance and distribution of TELPs (excess protons) between the liquid exposed areas of the Tf-Al-Tf membrane disk and septum that separates the anode and cathode liquid chambers.

Experiments		pH of Cathode Water	pH of Anode Water
With (Al-Tf-Al)	Before	6.89± 0.03	6.89± 0.03
200 V	After	5.78± 0.14	5.76± 0.09
With (Tf-Al-Tf)	Before	6.71± 0.10	6.71± 0.10
200 V	After	5.81± 0.04	5.76± 0.03
With (Al-Tf-Al)	Before	6.89± 0.03	6.89± 0.03
control (0V)	After	5.68± 0.06	5.78± 0.02
With (Tf-Al-Tf)	Before	6.71± 0.10	6.71± 0.10
control (0V)	After	5.76± 0.02	5.78± 0.04

Table 2. Averaged pH values that were measured in bulk water phase before and after 10 hours experimental run with "cathode water membrane water anode" systems. Adapted from Ref (Saeed and Lee, 2015) and (Saeed, 2016)

*The averaged pH values and standard deviation (± sign) were calculated from the original data of bulk water phase pH measurements.

cathode bulk water phase pH. As shown in *Table 2*, after the 10-hour experiment (200V) with the water Al-Tf-Al (membrane) water system, the measured pH value in the anode bulk water body (5.76± 0.09) remained essentially the same as that of the cathode bulk water phase (5.78± 0.14). These bulk water phase pH values averaged from 3 replication experiments (each replication experiment with at least 6 readings of pH measurement in each chamber water, n= 3 x 6 = 18) were statistically also the same as those (5.78± 0.04 and 5.76± 0.02) in the control experiments in the absence of the water electrolysis process (0V). This is a significant experimental observation since it confirmed the prediction of the TELPs model that the excess protons do not stay in the bulk water phase and thus cannot be measured by a pH electrode in the bulk phase.

Furthermore, the measured pH value of 5.76± 0.09 in the anode bulk water phase was also consistent with the observation that the piece of proton-sensing film placed in the anode bulk water phase (P_B) showed no sign of proton-associated Al corrosion activity while the proton-sensing film placed at P_I site had dramatic proton-associated Al corrosion (*Figures 3 and 4*). This indicated that the generated excess protons are localized primarily at the water-membrane interface at the P_I site resulting in a proton surface density that is high enough (pH < 3.8) to cause the aluminum corrosion there.

The pH measurements also showed that the freshly deionized water had an average pH value of 6.89± 0.03 before being used in the experiments (*Table 2*). Since the experiments were conducted with the laboratory ambient air conditions, the gradual dissolution of atmospheric CO_2 into the deionized water during a 10-hour experiment period resulted in water pH change from 6.89± 0.03 to 5.68± 0.06, which was observed in the control experiment with the same "cathode water Al-Tf-Al water anode" setup except without turning on the electrolysis voltage (0 V). Therefore, this bulk water pH change had little to do with the 200V-driven water electrolysis process. The same magnitude of bulk water pH change before and after the experiment was observed for the deionized water in both the anode and cathode chambers, which also supports the understanding that this bulk water pH change from the beginning to the end of the experiment was due to the gradual dissolution of atmospheric CO_2 into the deionized water during the 10-hour experiment period. There was no difference between the bulk-phase pH of anode chamber water (pH 5.76± 0.09) and that of

the cathode chamber water (5.78± 0.14) at the end of the experiment. This result also points to the same underlying understanding that the excess protons do not behave like typical solute molecules. Excess protons do not stay in the water bulk phase; they are transmembrane-electrostatically localized at the water-membrane interface at the P_I site so that they cannot be detected by the bulk-phase pH measurement

A further set of experiments with the setup of "cathode water Tf-Al-Tf water anode" was also conducted in triplicate. In this set of experiments, the Tf-Al-Tf membrane system was used instead of the Al-Tf-Al membrane system. Since the Teflon membrane is chemically inert to protons, the use of the Tf-Al-Tf membrane system eliminated the consumption of excess protons by the aluminum corrosion process at the P_I site that was demonstrated above. In this set of the experiments, no bulk-phase pH difference (ΔpH) between the anode and cathode water bodies was observed as well. As shown in *Table 2,* after 10 hours run at 200V with the "cathode water Tf-Al-Tf water anode" system, the measured pH value in the anode bulk water phase (5.76± 0.03) was essentially the same as that of the cathode bulk water phase (5.81± 0.04). This experimental observation again indicated that the excess protons do not stay in the bulk water phase and thus cannot be measured by the bulk liquid phase pH measurement. Since liquid water is an effective protonic conductor as discussed above, the excess protons produced in the anode water compartment are transmembrane-electrostatically localized to the water-membrane interface at the P_I site.

3. Induced TELP in an anode water-membrane-water-membrane-water cathode system

In the "anode water-membrane-water-membrane-water cathode" system illustrated in *Figure 6*, the anode water and cathode water in the ElectroPrep apparatus were concurrently electrolyzed at 200 V, forming excess protons / O_2 gas in the anode water chamber (P) and excess hydroxide anions / H_2 gas in the cathode (N) water chamber. Based on the TELPs model (Lee, 2012), it is predicted that the free excess protons in the anode chamber will migrate and localize themselves primarily at the water-membrane interface (the P site) in the anode (P) chamber. The excess protons localized at the P side will induce an electrostatic localization of hydroxide ions at the other

side of the membrane (the N' site) forming an "excess anions-membrane-excess protons" capacitor-like system (as shown on the right of the inset of *Figure 6)*. Similarly, the excess hydroxide ions generated in the cathode chamber will migrate and localize primarily at the water-membrane interface (the N site) in the cathode (N) chamber. It is predicted that this localization of hydroxide ions at the N side will induce the formation of TELPs at the other side of the membrane (the P' site) forming an "excess hydroxyl anions-membrane-induced protons water induced hydroxyl anions-membrane-excess protons" dual protonic capacitors (in-series) system (as shown in the inset of *Figure 6*).

These predicted features were indeed demonstrated through observation of TELPs activity on the Al films at the P and P' sites while there was no observable protonic activity at the N and N' sites, and no observable excess protonic activity in the bulk liquid phase at the P_B, C_B, and N_B sites in the three liquid chambers (*Figures 6 and 7*).

That is, as predicted, it was experimentally observed that the protonic sensing films (Al-Tf-Al) at the two ends of the Teflon sample chamber showed active protonic corrosion activity on P and P' sites adjacent with pure water (in absence of any salt) as shown in *Figures 6 and 7.*

It is worth mentioning that none of the Al films in the cathode water Al-Tf-Al water Al-Tf-Al water anode system could serve as an electrode since the Al films were not connected to any external voltage source. Each of the Al films acted solely as a protonic sensor and as part of a protonic insulating membrane in the three-water-chambers system as shown in *Figure 6*. That is, in this anode water-membrane-water-membrane-water cathode system, we also demonstrated an induced TELPs layer at the membrane-water interface (the P' site) in the center liquid chamber with the evidence of proton-sensing film at the P' site showing intense TELPs Al corrosion activity while those at C_B and N' sites showed no protonic Al corrosion activity (*Figure 7*).
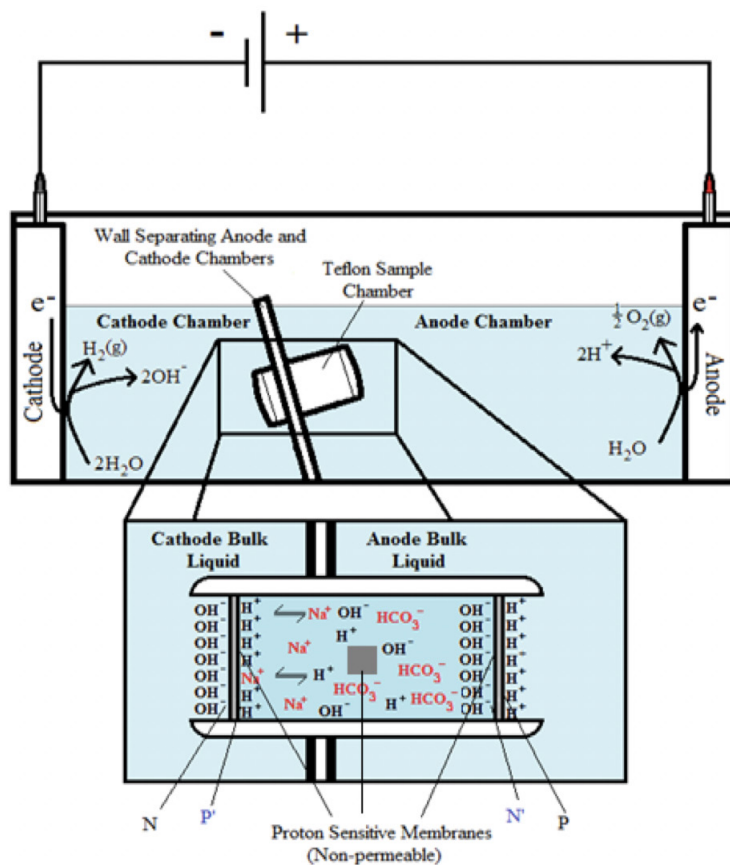

Figure 6. Schematic diagram of the system evaluating the effect of sodium cations on localized protons at the P' side in the Teflon center chamber. The inset shows the exchange of the added sodium (Na$^+$) cations with the electrostatically localized protons at the P' side. A small piece of proton-sensing Al film was placed into the bulk liquid phase (the C_B site) of the center chamber. Adapted from Ref (Saeed and Lee, 2018) and (Saeed, 2016).

As shown in *Table 3*, the bulk-phase pH measurements in the three-water-chambers system (*Figure 6*) also demonstrated that the Mitchellian proton delocalization view is not true. After the 10-hour water electrolysis (200 V), the measured pH value in the anode bulk water body (5.92 ± 0.12) remained nearly the same as that of the cathode bulk water phase (5.81 ± 0.07). If the Mitchellian proton delocalized view is true, there should be a significant bulk-phase pH difference (ΔpH) between the anode and the cathode water chambers; in contrast, the measured bulk pH data demonstrated again that the Mitchellian proton delocalized view is not true. These bulk water phase pH values averaged from 3 replication experiments (each replication experiment with at least 6 readings of pH measurement in each chamber water, n= 3 x 6 = 18) were statistically also the same as those (5.75± 0.08 and 5.77±
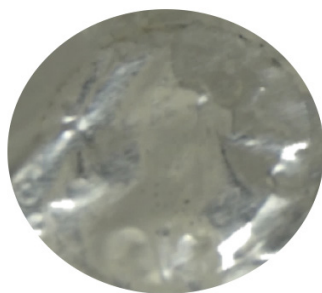
Proton-sensing film placed at cathode chamber (**N**) site.
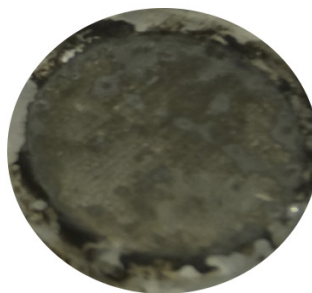
Proton-sensing film placed at the center Teflon chamber (**P'**) site.

Proton-sensing film placed at the center Teflon chamber (**N'**) site.

Proton-sensing film placed at anode chamber (**P**) site.

Proton-sensing film suspended inside the cathode bulk water phase (**N_B**)

Proton-sensing film suspended inside the anode bulk water phase (**P_B**)

Proton-sensing film was placed into the bulk liquid phase of the center chamber (**C_B**)

Figure 7. Observation of proton-sensing films after 10 hours electrolysis (200 V) for the cathode water-Al-Tf-Al-water-Al-Tf-Al-water anode experiment. Images show proton-sensing films that were placed at N, P, N', P', N_B, P_B and C_B sites. Adapted from Ref (Saeed and Lee, 2018) and (Saeed, 2016).

0.21) in the control experiments in absence of the water electrolysis process (0 V). Notably, these results again show that excess protons do not stay in the water bulk phase; they transmembrane-electrostatically localize at each of the P and P' sites so that they cannot be detected by the bulk-phase pH measurement.

These are significant observations, since both the protonic-sensing film detection and bulk liquid pH measurement have now demonstrated, for the first time, that protons can be localized at a water-membrane interface through electrostatic induction at the P' site in a "cathode water membrane (Al-Tf-Al) water membrane (Al-Tf-Al) water anode" system where the third water body (the center water chamber) is placed between an anode water chamber and a cathode water chamber interacting in series (*Figure 6*). The operation of this setup resulted in the formation of two protonic capacitors in series: a protonic capacitor across the membrane (Al-Tf-Al) with the N and P' sites and another one across the other membrane (Al-Tf-Al) with the N' and P sites as illustrated in *Figure 6*. This result again shows that liquid water bodies are protonic conductors; the behavior of excess protons in protonic conductors appears to be like that of excess electrons in electric conductors in forming capacitors across insulating membrane barriers.

4. Equilibrium constant of sodium cation (Na⁺) in exchanging with TELPs

Demonstration of TELPs at P' site in the center chamber enabled us to evaluate the cation exchange with TELPs by using salt solutions in the center chamber without requiring the use of salts in the anode and cathode chambers (*Figure 6*). Note, if salts are used in the anode and the cathode chambers, they might interfere with the electrolysis process and may complicate the interpretation of experimental data. Therefore, the discovery and utilization of induced TELPs at P' site in the center liquid chamber enabled us to perform quite clean experiments to determine the cation (Na⁺) exchange equilibrium constant with the induced TELPs without requiring the use of any salt in any of the anode chamber and the cathode chamber.

The cation-exchange experimental study (Saeed and Lee, 2018) showed that the addition of 10 mM and/or 25 mM sodium ions (sodium bicarbonate solution) in the center chamber had small effect on TELP density at the P' side facing the sodium salt solution, while the use of 75 mM sodium ions (in the center chamber) had substantial effect leading to the reduction of TELPs populations at the P' site approximately by about 50%, which was monitored by the color change of the proton-sensing Al film corrosion at the P' side in comparison with that of the proton-sensing film placed at the positive control (0 mM

Replicates	Experiment (200 V)			Control (0 V)		
	Cathode chamber pH	Center chamber pH	Anode chamber pH	Cathode chamber pH	Center chamber pH	Anode chamber pH
Replicate 1	5.88 ± 0.13	7.28 ± 0.18	5.82 ± 0.09	5.78 ± 0.14	5.91 ± 0.06	5.70 ± 0.08
Replicate 2	6.01 ± 0.09	7.04 ± 0.08	5.80 ± 0.01	5.75 ± 0.04	6.11 ± 0.05	5.89 ± 0.34
Replicate 3	5.85 ± 0.10	7.27 ± 0.14	5.79 ± 0.08	5.71 ± 0.03	6.17 ± 0.03	5.72 ± 0.10
Average	5.92 ± 0.12	7.20 ± 0.17	5.81 ± 0.07	5.75 ± 0.08	6.07 ± 0.13	5.77 ± 0.21

Table 3. Three replicates of final pH measurements for experiments with the "cathode water-Al-Tf-Al-water-Al-Tf-Al- water anode" system after 10 hours electrolysis (200 V) in comparison with the control (0 V). Adapted from Ref (Saeed and Lee, 2018) and (Saeed, 2016).

sodium ions: water with no salt) P' site and the Al film placed at the P site facing the anode liquid (also no salt). It required the use of 200 mM or higher sodium ion solution in the Teflon center chamber to exchange out the localized protons at the P' site to a level that could no longer be visually determined by use of a proton-sensing Al film (detection limit: about pH 3.8). Based on our analysis, this effect of sodium bicarbonate salt (NaHCO$_3$) solution on TELPs at the P' site is owing to the sodium cations being at higher concentrations (75 mM or above) that may partially exchange with TELPs at the P' site.

One might argue that the observed effect may be due to the bicarbonate anion and not due to the sodium cation. Therefore, the cation/TELPs exchange experiments (of different cation concentrations) were repeated with other cations such as K$^+$ that showed similar effect on the P' side (see the potassium cation/TELPs exchange experiments in the next section). Interestingly, in the K$^+$ salt solution, the 50% color density change at the P' site was observed at around 50 mM instead of 75 mM. This additional observation further supports that the observed effect was due to cation/TELPs exchange and not due to a bicarbonate effect. It is well known that the size of the potassium cation is bigger than the sodium cation. However, in aqueous solution as a free ion, the small sodium ion attracts more water molecules giving it a larger effective diameter compared to the hydrated potassium ion. Since the hydrated radius of the potassium ion is smaller than the hydrated radius of the sodium ion, its electro-diffusion mobility is faster compared to that of sodium. It was determined that the mobility of sodium ions under the influence of unit potential gradient (0.53 x 10^{-3} cm^2 V^{-1} s^{-1}) is slower than potassium ion mobility (0.76 x 10^{-3} cm^2 V^{-1} s^{-1}) under the same unit potential gradient (Eigen and De Maeyer, 1958). That may be one of the reasons why it required a higher concentration of sodium ions (75 mM) to delocalize 50% of TELPs on the P' site. Moreover, it was reported that fresh solutions of bicarbonate have no action on aluminum corrosion (Bell, 1962; Verdonik, 1999; Vargel, 2004; Scamans *et al.*, 2010).

The cation exchange equilibrium constant (K_p) can be expressed as:

$$K_p = \frac{[Na_L^+] \cdot [H^+]}{[H_L^+] \cdot [Na^+]} \qquad \text{(Equation 3)}$$

where [Na$_L^+$] is the localized sodium ions concentration at the water-membrane interface (P' site); [H$^+$] is the concentration of free delocalized protons in the bulk liquid

phase; [H$_L^+$] is the TELP concentration on the water-membrane interface (P' site); and [Na$^+$] is the free sodium ions concentration in the bulk liquid phase.

At the midpoint with 50-50% cation/TELPs exchange, the concentration of the localized non-proton cation would be equal to the concentration of TELPs. This means that when [Na$_L^+$] = [H$_L^+$], the cation exchange equilibrium constant (K_P) will be:

$$K_{pNa^+} = \frac{[H^+]}{[Na^+]} \qquad \text{(Equation 4)}$$

We observed that the 50-50% cation/TELPs exchange was achieved when the bulk liquid phase sodium ion concentration was 75 mM as indicated with a star sign (*) in *Table 4*. The pH of the sodium salt solution (75 mM) inside the Teflon center chamber before the sodium/proton exchange process was found to be 8.37 ± 0.09 as shown in *Table 3*. By using this pH value for the bulk proton concentration [H$^+$] and the known sodium ion concentration (75 mM) in Equation 4, the sodium/TELPs exchange equilibrium constant was calculated to be 10$^{-(8.37 \pm 0.09)}$ M /0.075 M= (5.86 ± 1.2) x 10^{-8}.

We noticed that the pH of the sodium ion solution (75 mM) was somewhat increased during the cation-TELPs exchange experiment using the Al film-based protonic sensor (Equation 2) at the P′ site. The final pH value of the bulk sodium bicarbonate solution after 10 hours experimental run at 200V was 8.48 ± 0.07. Using this final pH value (8.48 ± 0.07) for the bulk proton concentration [H$^+$] and the known sodium ion concentration (75 mM) in Equation 4, the K$_{pNa+}$ value was calculated to be 10$^{-(8.48 \pm 0.07)}$ M /0.075 M= (4.45 ± 0.73) x 10^{-8}, which is slightly smaller than that calculated using the initial pH (8.37 ± 0.09). The true value of the sodium/TELPs exchange equilibrium constant K$_{pNa^+}$ is likely to be between [(5.86 ± 1.2) x 10^{-8} and (4.45 ± 0.73) x 10^{-8}], which gives an average of (5.07 ± 0.97) x 10^{-8}.

Using the averaged sodium/TELPs exchange equilibrium constant K$_{pNa^+}$ of (5.07 ± 0.97) x 10^{-8}, we have now calculated the %TELP density as a function of bulk liquid phase sodium concentration [Na$^+$] and bulk liquid phase proton concentration [H$^+$] (that can be calculated from the bulk liquid pH) using the following equation:

$$\% TELP\ density = \frac{100\%}{1+(K_{pNa^+}[Na^+]/[H^+])} \qquad \text{(Equation 5)}$$

Table 4 lists the percentage (%) of TELP density calculated for a series of sodium bicarbonate (NaHCO$_3$) salt solution

concentrations [Na⁺] in a range from 0 to 500 mM inside the Teflon center chamber. This calculation employed the averaged sodium/TELPs exchange equilibrium constant K_{pNa^+} of $(5.07 \pm 0.97) \times 10^{-8}$, and bulk liquid phase proton concentration [H⁺] that was calculated from the initial bulk liquid pH (10 hours 0V), the final bulk liquid pH (10 hours 200V of water electrolysis), or the averaged pH of 8.43 at the midpoint sodium bicarbonate concentration (75 mM).

Figure 8 presents a plot of the sodium cation/TELPs exchange data listed in *Table 4* on the percentage (%) of TELP density calculated through Equation 5 from the initial bulk liquid pH (10 hours 0V), the final bulk liquid pH (10 hours 200V), and the averaged cation-TELPs exchange midpoint sodium bicarbonate (75 mM) solution pH 8.43, using the averaged cation/TELPs exchange equilibrium constant K_{pNa^+} of $(5.07 \pm 0.97) \times 10^{-8}$ for liquid phase sodium concentrations [Na⁺] in a range from 0 to 0.5 M. The data plot shows a clear trend of TELP density reduction from 100% TELP to around 20% as the liquid phase sodium solution concentrations [Na⁺] gradually increased from 0 M to 0.5 M, which is clearly in a good qualitative agreement with the predicted feature of cation exchange with TELPs.
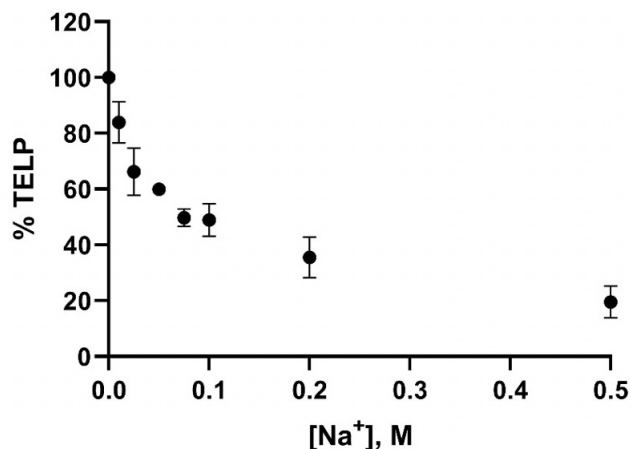

Figure 8 shows a plot of the percentage (%) of TELP density calculated through Equation 5 using the initial liquid pH (10 hours 0V), the final liquid pH (10 hours 200V), and the averaged liquid phase pH of 8.43 at the cation-TELPs exchange midpoint sodium bicarbonate concentration (75 mM), using the averaged sodium/TELPs exchange equilibrium constant K_{pNa^+} of $(5.07 \pm 0.97) \times 10^{-8}$ for liquid phase sodium concentrations [Na⁺] in a range from 0 to 0.5 M.

5. Equilibrium constant of potassium cation (K⁺) in exchanging with TELPs

Similarly, as previously reported (Saeed, 2016; Saeed and Lee, 2018) and listed in *Table 5*, it was experimentally determined that at 50 mM potassium ion concentration (the midpoint), the %TELP density on the proton sensi-

[Na⁺]	Initial pH (10 hours 0V)	Final pH (10 hours 200V)	%TELP calculated from initial liquid pH	%TELP calculated from final liquid pH	%TELP calculated from midpoint liquid pH
0 mM	6.41 ± 0.03	7.52 ± 0.02	100	100	100
10 mM	8.42 ± 0.01	8.81 ± 0.05	88	75	88
25 mM	8.61 ± 0.24	8.76 ± 0.11	66	58	75
50 mM	8.39 ± 0.02	8.45 ± 0.02	62	58	60
75 mM*	8.37 ± 0.09	8.48 ± 0.07	53	47	50
100 mM	8.22 ± 0.02	8.30 ± 0.01	54	50	43
200 mM	8.16 ± 0.01	8.19 ± 0.03	41	39	27
500 mM	8.11 ± 0.02	8.14 ± 0.01	23	22	13

Table 4. Sodium cation/TELPs exchange data on the percentage (%) of TELP density calculated for a series of sodium bicarbonate ($NaHCO_3$) salt solution concentrations [Na⁺] in a range from 0 to 500 mM inside the Teflon center chamber, using the averaged sodium/TELPs exchange equilibrium constant K_{pNa^+} of $(5.07 \pm 0.97) \times 10^{-8}$, and bulk liquid phase proton concentration [H⁺] that was calculated from the initial bulk liquid pH (10 hours 0V), the final bulk liquid pH (10 hours 200V of water electrolysis), or the averaged pH of 8.43 at the midpoint sodium bicarbonate concentration (75 mM). Adapted from Ref (Saeed and Lee, 2018) and (Saeed, 2016).

*pH measurement for 75 mM sodium bicarbonate (midpoint with 50-50% sodium/proton exchange) is average of 4 replications while the rest of pH measurements are averages of 2 replications.

tive membrane was decreased to about half compared to that of the control in the absence of potassium ion (0 mM). The pH of the potassium salt solution (50 mM) inside the Teflon center chamber before the potassium/proton exchange process was determined to be 8.45 ± 0.03. By using this pH value for the bulk liquid phase proton concentration $[H^+]$ and the known potassium ion concentration (50 mM) in the following equation:

$$K_{pK^+} = \frac{[H^+]}{[K^+]}$$ (Equation 6)

the potassium/TELPs exchange equilibrium constant was calculated to be $10^{-(8.45 ± 0.03)}$ M /0.050 M= (7.20 ± 0.59) x 10^{-8}.

The final pH value of the bulk potassium bicarbonate solution after a 10-hour experimental run at 200V of water electrolysis was 8.48 ± 0.13. Using this final pH value (8.48 ± 0.13) for the bulk liquid proton concentration $[H^+]$ and the known potassium ion concentration (50 mM) in equation 6 the K_{pKa^+} value was calculated to be $10^{-(8.48 ± 0.13)}$ M /0.050 M= (6.85 ± 1.99) x 10^{-8}, which is slightly smaller than that calculated using the initial pH (8.45 ± 0.03). The true K_{pKa^+} value is likely to be in between (7.20 ± 0.59) x 10^{-8} and (6.85 ± 1.99) x 10^{-8} with an average of (6.93 ± 1.23) x 10^{-8}.

Note that the bulk concentration of potassium ions after the potassium/proton exchange process used in determining the potassium cation exchange equilibrium constant was the same as the given initial potassium bicarbonate solution concentration that resulted in a 50-50%
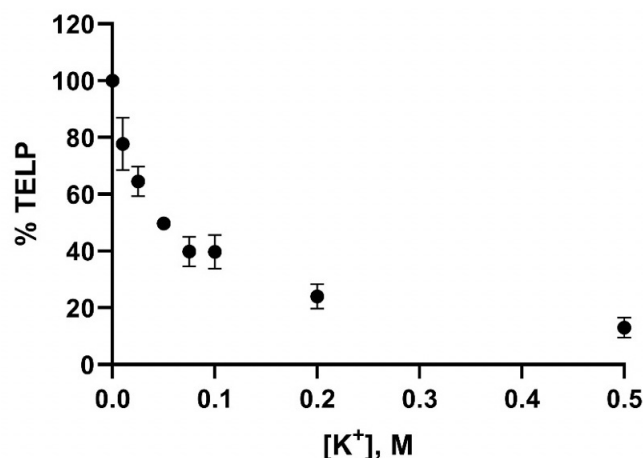

Figure 9 shows a plot of potassium cation/TELPs exchange data on the percentage (%) of TELP density calculated through Equation 5 using the initial liquid pH (10 hours 0V), the final liquid pH (10 hours 200V), and the averaged liquid phase pH of 8.47 at the cation-TELPs exchange midpoint potassium bicarbonate concentration (50 mM), using the averaged potassium/TELPs exchange equilibrium constant K_{pKa^+} of (6.93 ± 1.23) x 10^{-8} for liquid phase potassium concentrations $[K^+]$ in a range from 0 to 0.5 M.

$[K^+]$	Initial pH (10 hours 0V)	Final pH (10 hours 200V)	%TELP calculated from initial liquid pH	%TELP calculated from final liquid pH	%TELP calculated from midpoint liquid pH
0 mM	6.79 ± 0.07	7.86 ± 0.16	100	100	100
10 mM	8.47 ± 0.05	8.85 ± 0.08	83	67	83
25 mM	8.42 ± 0.03	8.61 ± 0.11	69	59	66
50 mM*	8.45 ± 0.03	8.48 ± 0.13	51	49	50
75 mM	8.37 ± 0.03	8.56 ± 0.03	45	35	40
100 mM	8.30 ± 0.01	8.26 ± 0.03	42	44	33
200 mM	8.26 ± 0.01	8.36 ± 0.01	28	24	20
500 mM	8.19 ± 0.01	8.23 ± 0.03	16	15	9.0

Table 5. Potassium cation/TELPs exchange data on the percentage (%) of TELP density calculated through Equation 5 for a series of potassium bicarbonate ($KHCO_3$) salt solution concentrations $[K^+]$ in a range from 0 to 500 mM inside the Teflon center chamber, using the averaged sodium/TELPs exchange equilibrium constant K_{pKa^+} of (6.93 ± 1.23) x 10^{-8}, and bulk liquid phase proton concentration $[H^+]$ that was calculated from the initial bulk liquid pH (10 hours 0V), the final bulk liquid pH (10 hours 200V of water electrolysis), or the averaged pH of 8.47 at the midpoint potassium bicarbonate concentration (50 mM). Adapted from Ref (Saeed and Lee, 2018) and (Saeed, 2016).

*pH measurement for 50 mM potassium bicarbonate (midpoint with 50-50% potassium/proton exchange) is average of 4 replications while the rest of pH measurements are averages of 2 replications.

cation/TELPs exchange (*i.e.*, 50 mM K$^+$). This is because the amount of TELPs that was exchanged out by the potassium ions was likely to be so small that it would not significantly reduce the 50 mM K$^+$ concentration.

Figure 9 presents a plot of the potassium cation/TELPs exchange data listed in *Table 5* on the percentage (%) of TELP density calculated through Equation 5 from the initial bulk liquid pH (10 hours 0V), the final bulk liquid pH (10 hours 200V), and the averaged cation-TELPs exchange midpoint potassium bicarbonate (50 mM) solution pH 8.47, using the averaged potassium/TELPs exchange equilibrium constant K_{pKa}^+ of (6.93 ± 1.23) x 10^{-8} for liquid phase potassium concentrations [K$^+$] in a range from 0 to 0.5 M. The data plot shows a clear trend of TELP density reduction from 100% TELP to about 15% as the liquid phase potassium solution concentrations [K$^+$] gradually increased from 0 M to 0.5 M, which is clearly in a good qualitative agreement with the predicted feature of cation exchange with TELPs.

6. Discussion and Commentary in Responding to Silverstein's Arguments

From the experimental results as reviewed above, readers can now see that the experimental demonstration of TELPs was accomplished through: 1) using an aluminum film as a TELPs sensor in a biomimetic anode water-membrane-water cathode system (*Figures 1-4*); 2) analyzing the water-electrolysis current curve (*Figure 5* and *Table 1*); and 3) measuring bulk liquid phase pH (*Table 2*). Furthermore, the formation of induced TELPs was discovered on the P' site membrane surface at the left end of the central liquid chamber in an anode water-membrane-water-membrane-water cathode system (*Figures 6 and 7* and *Table 3*). The discovery of induced TELPs enabled a clean experimental test for the cation-TELPs exchange process by using sodium bicarbonate or potassium bicarbonate solution in the central liquid chamber (*Figure 7*). Each of the sodium and potassium cation-TELPs exchange equilibrium constants was determined by identifying the midpoint of the cation-TELPs exchange. The sodium/TELPs exchange equilibrium constant K_{pNa}^+ is likely to be between ((5.86 ± 1.2) x 10^{-8} and (4.45 ± 0.73) x 10^{-8}), which gives an average of (5.07 ± 0.97) x 10^{-8}. The potassium/TELPs exchange equilibrium constant K_{pKa}^+ is likely to be between (7.20 ± 0.59) x 10^{-8} and (6.85 ± 1.99) x 10^{-8} with an average of (6.93 ± 1.23) x 10^{-8}. Further analy-

sis (*Tables 4 and 5; Figures 8 and 9*) affirmed that the experimental TELP demonstration and the cation-TELPs exchange equilibrium constant values are valid. Many of Silverstein's arguments appear to stem from his own misunderstanding, such as his misconception on the Al film protonic sensing limit. The four major arguments from Silverstien 2024 are hereby addressed as follows:

Protonic Al corrosion is distinct from hydroxide anions Al corrosion.

It is commonly known that aluminum (Al) material is sensitive to acids (protonic Al corrosion) and base (hydroxide anions corrosion), which represent two distinct corrosion processes. According to the analysis of the potential-pH diagram for pure Al at 25˚C in aqueous solution shown in *Figure S1* (adapted from Pourbaix 1974) using the Web-PlotDigitizer software tool (Rohatgi, 2024), the required pH value (proton concentration) to enable protonic Al corrosion is a high proton concentration that is equivalent to a pH value of less than 3.8. In contrast, the hydroxide anions Al corrosion requires an alkaline pH larger than pH 8.6.

Therefore, readers may now also be able to understand that Silverstein seems to have completely "mixed up" the protonic Al corrosion with the hydroxide anions Al corrosion, as judging from his argument (I) "The dark stains on the Al film, interpreted as proton-induced 'corrosion' are chemically unidentified, and are seen above pH 8.7 (in control experiments in the absence of electrolysis). Hence, they may have nothing to do with proton-sensing."

As shown in the Supporting Information (*Figure S2*) of the 2018 Saeed and Lee report (Saeed and Lee, 2018), the alkaline (hydroxide anions) Al corrosion stain in the Al film looks yellowish, which is qualitatively different from the stain of the protonic Al corrosion that looks more or less dark whitish grey. That is, the hydroxyl anions-based Al corrosion is a completely different process that shall not be confused with the protonic (TELPs) Al corrosion that requires high effective proton concentration with pH < 3.8.

Furthermore, as shown in Equation 2, the primary product of the protonic Al corrosion is Al^{3+} ion, which could interact with water and be converted (by binding with hydroxide anions from water nearby) to the gelatinous aluminum hydroxide (Al(OH)$_3$) precipitate on Al film surface. This protonic Al corrosion was employed as TELPs

sensing indicator in the experimental demonstration of TELPs formation, in addition to other analytic techniques including the electrolysis current measurements and the bulk liquid phase pH measurements.

The cation-TELPs exchange equilibrium constant values are now further analyzed to be valid.

In contrast to Silverstein's wild claim (II) "The ion exchange equilibrium constant values are wrong by several orders of magnitude", the experimentally demonstrated TELPs and the subsequently measured Na$^+$ (and K$^+$) -TELPs exchange equilibrium constant values are now further analyzed to be valid.

We understand that Silverstein's claim apparently was from his misconception about the TELPs detection limit of protonic sensing Al films. In our early publications (Saeed and Lee, 2015; Saeed, 2016; Saeed and Lee, 2018), it has been made abundantly clear to readers that the protonic Al corrosion sensing requires a relatively high proton concentration that should be at least above 0.1 mM (pH below 4). For an example, in the Saeed and Lee 2015 publication (Saeed and Lee, 2015) that Silverstein has cited in his 2024 article (Silverstein, 2024b), we have clearly stated: "It is known that aluminum surface can begin to be corroded by protons when the effective proton concentration is above 0.1 mM (equivalent to a pH value below 4) (Pourbaix, 1974a; Pourbaix, 1974b). This property was therefore employed as a proton-sensing mechanism in combination with the bulk phase pH electrode measurement to determine the distribution of excess protons in the water-membrane-water system."

This information about Al film protonic detection limit (pH 3.8) is provided also in the Supporting Information (*Figure S1*) of the Saeed and Lee 2018 publication (Saeed and Lee, 2018) that Silverstein cited in his 2024 article (Silverstein, 2024b). Unfortunately, Silverstein either overlooked or neglected this important piece of information on the protonic Al corrosion-based detection limit of about pH 3.8, so that he wrongly assumed the Al film

protonic detection limit observed with 200 mM Na$^+$ as to be "$f_{H+} \approx 0$" (*i.e.*, 0% TELP) in his "curve fitting" shown in his 2024 article's "Figure 1"; that apparently gave him completely wrong calculations from which he wrongly claimed "K_{eq} for surface ion exchange to be 9 to 37 times higher" (Silverstein, 2024b).

In his 2024 article's "Figure 1," only the curve with our previously determined cation/TELPs exchange equilibrium constant K_{pNa^+} of 5.05 x 10^{-8} that predicts 24±10 % TELP at 200 mM Na$^+$ is in line with the trend of our experimental data (*Figure 8*). Using the predicted 24±10 % TELP as shown in *Table 6*, we calculated the projected TELP density to be (2.04 ± 0.57) ×10^{-4} M, which is equivalent to a TELP pH of 3.72 ± 0.14 that well matches the protonic Al film corrosion detection limit of about pH 3.8. Therefore, the analysis results here have further affirmed that the experimental TELP demonstration and the experimentally determined cation-TELP exchange equilibrium constant values are valid.

Biomimetic systems like the anode water-membrane-water cathode system are valuable for TELPs capacitor demonstration and study at the present time.

Readers may now understand that biomimetic systems like the anode water-membrane-water cathode system (*Figure 1*) are valuable for TELP capacitor demonstration and scientific study, in contrast to Silverstein's argument (III) "The water electrolysis system is not 'biomimetic,' and the expectation that this aqueous Al-Tf-Al disk system behaves like a capacitor-containing electrical circuit seems unlikely" (Silverstein, 2024b).

Using the biomimetic systems as shown in *Figures 1, 2, 4 and 6*, protonic capacitors with TELPs have been well demonstrated. Formation of induced TELPs is discovered (*Figures 6 and 7*). The sodium and potassium cation-TELP exchange equilibrium constants have been experimentally determined by neatly evaluating the effects of bicarbonate salts on induced TELPs in the central liquid chamber (*Figures 8 and 9*).

	TELP density (M)	TELP pH
(24−10) % of TELP	1.19×10^{-4}	3.92
24 % of TELP	2.04×10^{-4}	3.69
(24 +10) % of TELP	2.89×10^{-4}	3.54
Average ± Std	(2.04 ± 0.57) ×10^{-4}	3.72 ± 0.14

Table 6. Projected TELP density and TELP pH when the TELP density is reduced to 24±10% of 8.49×10^{-4} M (from *Table 1*).

WATER

Recently, Silverstein in his critique (Silverstein, 2023) made another interesting comment: "It seems a stretch to claim that foil covered Teflon® is a 'biomimetic' membrane: Both Teflon® (polytetrafluoroethylene) and the metal/water surface are hydrophobic, whereas lipid head groups at the membrane surface are polar. Thus, there is no reason to expect the structure of water at Lee's Teflon®/Al foil surface to resemble that at the lipid bilayer membrane surface." We do not think that would be much of an issue. The TELPs model (Lee, 2019a; Lee, 2020b; Lee, 2023a; Lee, 2023d; Lee, 2024a) has already indicated that a protonic capacitor forms across the <u>hydrophobic</u> alkane core membrane and lipid head groups have little to do with TELPs. That is, the TELPs model treats a proton-impermeable membrane as an insulator, which is in the same way as how our bioenergetics founding father Peter Mitchell had done in his pioneering Chemiosmotic Theory (Mitchell, 1985; Mitchell and Moyle, 1967).

Silverstein's claim "the Teflon® disk employed by Saeed and Lee is much too thick to serve as a capacitor holding excess charge in the water surface layers on opposite sides of the disk" (Silverstein, 2024b) is also unfounded. That claim was apparently due to his own mistake in calculating the transmembrane attractive force for a protonic capacitor. Silverstein improperly used his "Bjerrum length" argument (Knyazev et al., 2023; Silverstein, 2024a) through which, in his words, "the electrostatic energy of attraction between a [single] H$^+$/OH$^-$ pair separated by a dielectric medium of thickness r can be calculated from Coulomb's Law" (Silverstein, 2024b) that substantially underestimates the true transmembrane attractive force that is contributed by multiple transmembrane electrostatic interactions.

For example, when a membrane thickness of 75 μm is used as in a biomimetic Teflon membrane protonic capacitor (Saeed and Lee, 2015), a transmembrane-electrostatically localized H$^+$ (TELP) charge will be able to electrostatically interact with huge numbers of transmembrane-electrostatically localized HO$^-$ anions (TELAs). For instance, with a bird's eye view angle of 45 degrees from a membrane surface, each proton will be able to electrostatically "see" through the 75-μm thick Teflon membrane for the HO$^-$ anions at the other side of the membrane within an area as large as 18000 μm^2 [= 3.14 x (75 μm)^2]. For a 75-μm thick biomimetic Teflon membrane with a TELC density of 5600 electronic charges/μm^2, the number of transmembrane-electrostatically localized HO$^-$ anions that each transmembrane-electrostatically localized pro-

ton can electrostatically interact with is now estimated to be about 10^8. Therefore, the "Bjerrum length" argument that Silverstein with Pohl's group repeatedly used (Silverstein, 2024a; Silverstein. 2024b; Zhang et al., 2012) could fail to account for the protonic transmembrane attractive force from as many as 10^8 TELP-TELA electrostatic interactions for each of the transmembrane-electrostatically localized H$^+$ charges. Readers can now see how the improper application of the Bjerrum length argument by Silverstein (Silverstein, 2024a; Silverstein, 2024b; Zhang et al., 2012) to a biomimetic Teflon membrane with a thickness of 75 μm could result in immense analysis errors off by orders of magnitudes.

Note that the electric field strength across a 75-μm Teflon membrane protonic capacitor equilibrated with 200 V of water electrolysis voltage was calculated to be 2.67 x 10^{+6} V/m, which is equivalent to that of a biological membrane potential of about 10 mV (across a typical 4-nm thick biomembrane). Therefore, the biomimetic studies (Saeed, 2016; Saeed and Lee, 2015) provided a reasonable biomimetic experimental demonstration of TELPs. Based on the protonic capacitance of the Teflon membrane (thickness 75 μm) employed in the experiment with an electrolysis voltage of 200 V, we calculated that the steady state TELP concentration at the Teflon membrane-liquid interface is likely to be about 0.51 mM, which is equivalent to a local pH of 3.3 that an Al film can readily sense. This calculated result is in line with the experimentally estimated TELP density of 8.49×10^{-4} M (0.85 mM) H$^+$ (equivalent to a localized pH value of 3.07) as listed in $Table$ 1. Therefore, the calculated result based on the Teflon membrane protonic capacitance is in good qualitative agreement with the dramatic protonic corrosion activity observed on the Al film placed at the positive liquid-membrane interface (P$_I$) in the experiments ($Figures$ 3 and 4).

The experimental demonstration of TELPs rejects the putative "potential well/barrier model."

In contrast to Silverstein's argument (IV), "Saeed and Lee's rejection of the alternative barrier models for proton surface localization is unfounded," our successful experimental demonstration of TELPs indeed rejects the putative "potential well/barrier model" whose "potential well" was claimed to have a negative ΔG "for the depth of the potential well near the interface (4–8 RT at 1–2 Å)" and whose "activation barrier" height was claimed to be as high as "ΔG^{o‡} ≈ 20–30 RT" (Silverstein, 2023). We found problematic issues with the putative "potential well/barrier model" (Silverstein, 2023) that could not really explain

protonic bioenergetics and/or experimental observations.

First of all, Silverstein's claimed "$\Delta G^{o\ddagger} \approx$ 20–30 RT " (+ 25 RT ?) in the liquid water phase at the location of 0.4 nm away from the hydrophobic surface (Silverstein, 2023) would be equivalent to an activation barrier of about 60.9 kJ/mol; that is likely to be questionable since he has never explained how could it be possible for water molecules to form such a high activation barrier that is far higher than their hydrogen bond energy. According to an independent study (Markovitch and Agmon, 2007), the water hydrogen bond Gibbs energy ΔG^0 is 2.7 kJ/mol (with ΔH^0 = 7.9 kJ/mol and $T\Delta S^0$ = 5.2 kJ/mol). For the mechanism of proton mobility, the activation energy E_A is reported to be 11.3 kJ/mol (Lapid *et al*., 2004; Markovitch and Agmon, 2007), in contrast to Silverstein's claimed "$\Delta G^{o\ddagger} \approx$ 20–30 RT " (around 60.9 kJ/mol).

Second, even if assuming the putative "potential well/barrier" model would be true, it still could not explain the relevant bioenergetics. As shown in Silverstein's 2023 article, the bottom of the putative Gibbs free energy potential well (−6 $RT,$ if true) would be located about 0.15 nm away from the hydrophobic surface; the peak of the activation barrier (+25 $RT,$ if true) would be located at 0.4 nm away from the hydrophobic surface. Consequently, if the "potential well/barrier" model were correct, it would imply that the protonic outlet of mitochondrial proton pumps would have been located precisely inside the "potential well" that would be within 0.4 nm from the alkane surface of the membrane. Otherwise, the protonic outlet (that protrudes into the liquid phase at least about 1 nm away from the hydrophobic core membrane surface) will be outside the putative "potential well/barrier." If the protonic pump outlet protrudes more than 0.6 nm away from the hydrophobic core membrane surface (so that it is outside the putative potential well/barrier), the "potential well/barrier" model (even if it exists) would not work. The reality is that many known protonic pump outlets such as those of complexes I, III and IV in mitochondria apparently protrude into the liquid phase at least 1-3 nm away from the membrane surface (Dudkina *et al*., 2010; Lee, 2021b; Lee, 2023b; Lee, 2024a; Lee, 2024b); they thus do not support the "potential well/barrier model." Therefore, it is again quite clear that the putative "potential well/barrier model" as proposed by Junge and Mulkidjanian (Cherepanov *et al*., 2003; Mulkidjanian *et al*., 2006) and advocated by Silverstein (Silverstein, 2023) does not really exist, or the putative potential well/barrier (even if

it exists) is irrelevant to explaining the real world protonic bioenergetics.

Furthermore, based on Silverstein's comment, "both Teflon® (polytetrafluoroethylene) and the [Al] metal/water surface are hydrophobic" (Silverstein, 2023), which we can all agree with, then the "potential well/barrier model" would predict that all the Al films placed in the anodic water chamber would trap the excess protons by the "potential well" of "(4–8 RT at 1–2 Å)." Thus, if the "potential well/barrier model" were true, all the Al films in contact with the anode water would have displayed protonic Al corrosion by the excess protons, regardless of whether the Al films were placed in the anode chamber bulk liquid (P_B), on the surface of the chamber bulk liquid (P_S), or at the P_I site to serve as part of the membrane for protonic capacitor formation (*Figure 1*). In stark contrast to the "potential well/barrier model" prediction, the experimentally observed fact shows that only the Al film that was placed at the P_I site to serve as part of the membrane for protonic capacitor formation showed dramatic protonic Al corrosion (*Figure 4*); all the other Al films, including the one that was placed in the bulk liquid (P_B) and the one that floated on the anode liquid water surface (P_S), showed no sign of any protonic Al corrosion (*Figures 1, 2, and 3*). Therefore, the experimental results (*Figures 1-4*) clearly demonstrated TELP protonic capacitor formation as predicted by the TELPs model and rejected the putative "potential well/barrier model." That is, the putative "potential well/barrier model" as proposed by Junge and Mulkidjanian (Cherepanov *et al*., 2003; Mulkidjanian *et al*., 2006) and advocated by Silverstein (Silverstein, 2023) does not really exist, or the putative potential well/barrier (even if it exists) is irrelevant to explaining the experimental observations in the demonstration of TELPs formation (*Figures 1-4*).

7. Call for future research on more direct detection of TELC activities

Notably, excess protons have been reported in water with excess electric charge (Fuchs *et al*., 2016; Santos *et al*., 2011). Based on the TELC theory (Lee, 2019a; Lee, 2020b; Lee, 2021b) with liquid water as protonic conductor, it is expected that the excess protons will appear on the liquid water surface because of the mutual repulsion of excess protons that is known also as the Gauss law effect of electrostatics (Lee, 2012; Lee, 2023b; Lee, 2023d). This feature as expected was also shown by indepen-

dent studies where the migration of excess protons to the liquid/air interface has been simulated (Petersen and Saykally, 2005) and observed experimentally (Fuchs *et al*., 2019).

The author (Lee) hereby encourages the scientific community and research funding agencies to increase their research efforts into further detection and verification of TELC activities in both biomimetic systems and cellular membrane systems. In the work reviewed in the present paper, TELP activities were directly detected through the TELP-enabled Al corrosion observed in a pure anode water-membrane-water cathode system (*Figures 1-5*). Subsequently, we were even able to manipulate the TELP activities through the cation-proton exchange process by adding salts, including sodium bicarbonate or potassium bicarbonate in the liquid phase (*Figures 6-9*). Therefore, the experimental protonic capacitor demonstration with direct TELP detection and manipulation is now accomplished well beyond any reasonable doubt. Owing to the paramount significance of the TELC theory (Lee, 2019a; Lee, 2020b; Lee, 2021b) to better the fundamental understanding of bioenergetics, neuroscience, and life systems in general, more direct experimental evidences of TELC/TELP activities, such as local pH changes, proton transport visualization by, e.g., Raman spectroscopy, pH distribution analysis using dyes or other chemical tracers, are still highly desirable.

According to our understanding with the TELC model (Lee, 2019a; Lee, 2020b; Lee, 2021b), TELC/TELP activities are likely to be dynamic. Although they are in dynamic communication with the bulk aqueous liquid phase through the cation-proton exchange process, most of the TELPs are likely to stay in the first layer of water molecules on the hydrophobic core membrane surface that is beneath the membrane's lipid head groups. So far, there are no known artificial pH sensor that could be used to directly observe TELPs in biological membrane systems. This could probably explain why TELPs were not noticed for more than a half century since the "delocalized vs. localized proton coupling" debates that began in the 1960s. This also shows the importance now to develop and employ a new type of protonic sensors to directly observe TELPs within the first layer of water molecules on hydrophobic core membrane surface in biological membrane systems. Based on our current knowledge, there are at least two natural membrane protein complexes that can sense and use TELPs: the F_oF_1-ATP synthase (Lee, 2023b) and the melibiose transporter MelB (Hariharan *et al*.,

2024). Researchers are highly encouraged to take their cue and inspiration from the natural TELPs-sensing biomolecules to better design and make the needed protonic probes for more direct detections of TELPs in biomembrane systems.

Acknowledgments

Author Information

Corresponding Author

*James Weifu Lee. Department of Chemistry and Biochemistry, Old Dominion University, Norfolk, VA 23529 United States, Email: jwlee@odu.edu, Tel: 757-683-4260

Author Contributions

Lee designed and performed research, analyzed data, and authored the paper.

Funding Declaration

Competing Interests

The author has declared that no competing interests exist.

Data availability

All data generated or analyzed during this study are included in this article and in the cited references.

Experimental demonstrations of transmembrane-electrostatically localized protons prevail

Known information on the (acids) protonic aluminum (Al) corrosion and the (base/alkaline) hydroxide anions Al corrosion

Based on the analysis of the potential-pH diagram for pure Al at 25˚C in aqueous solution shown in *Figure S1* (adapted from Pourbaix, 1974) using the WebPlotDigitizer software tool (Rohatgi, 2024), the required pH value (proton concentration) to enable protonic Al corrosion is a relatively high proton concentration that is equivalent to a pH value of less than about pH 3.8. For hydroxyl ion Al corrosion, the required pH (hydroxyl anion concentration) is larger than pH 8.6.

Corrosion of Aluminum in an aqueous environment is governed mainly by two crucial factors: the pH of the solution (the surrounding environment) and the applied voltage (Pourbaix, 1974a; Pourbaix, 1990; Scamans *et al.*, 2010; Talbot, 1998). The thermodynamic principles that control the corrosion of Aluminum could be better understood by the Pourbaix (Potential-pH) diagram, which is a graphical representation of solid phases and soluble ions of the Al metal that are produced electrochemically
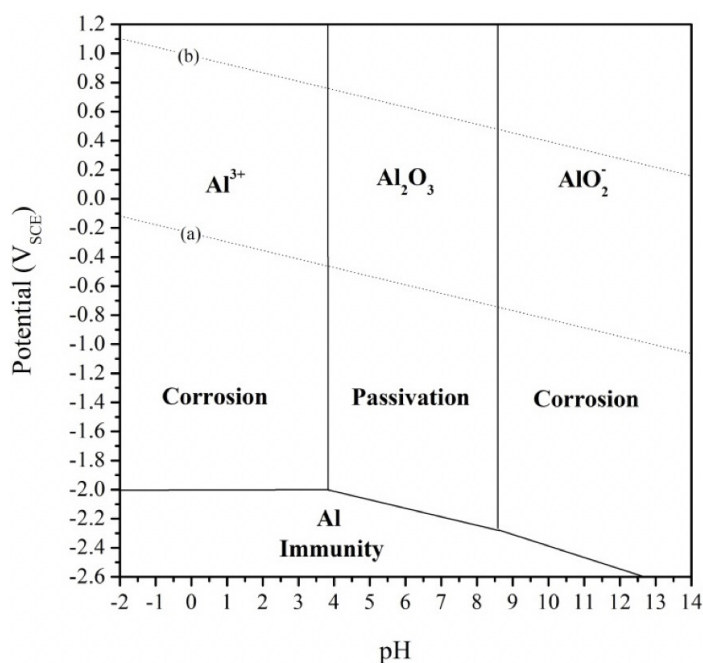

Figure S1. Potential-pH diagram for pure Al at 25˚C in aqueous solution (adapted from Pourbaix, 1974). The lines (a) and (b) correspond to water stability and its decomposed product (Sukiman *et al.*, 2012). Adapted from Ref (Saeed and Lee, 2015) and (Saeed, 2016).

(*Figure S1*). *Figure S1* shows that there are three possible states of the Al in aqueous solution:

1) Corrosion region in which Al metal is vulnerable to corrosion and becomes stable in its ionic (soluble) product when the pH of the surrounding environment is below 3.8 or above 8.5 and the potential is above -2.0 V versus SCE (Standard Calomel Electrode). In an acidic environment (< pH 3.8), aluminum oxidizes forming Al^{3+} soluble ions while in an alkaline environment (> pH 8.5) aluminum forms AlO_2^- that is soluble in aqueous phase.

2) Passive region in which the Al metal tends to be protected by a coating of Al oxide that is a passive layer that acts as a barrier between Al metal and the surrounding environment, thus preventing any contact between the metal and the environment. This passive layer is stable when the pH of the surrounding is in between 4 and 8.5.

3) Immunity region in which the Al metal is immune from corrosion attack. This region is achieved when the potential of the metal is kept below -2.0 V versus SCE.

Additional responses from Lee to Silverstein's comments:

Silverstein: *(I) Saeed and Lee did not account for the possibility that a significant fraction of Al oxidation could be due to reaction with dissolved oxygen.*

Lee Response: The "dissolved oxygen" is available to all pieces of Al films, including those of both the TELP experiments (200 V = water electrolysis excess proton production) and the control experiments (0V = no water electrolysis = no excess proton production). According to the Silverstein argument here, all pieces of Al films would have the corrosion stain, which clearly was not the case. The experimentally observed fact shows that only the Al film that was placed at the P_l site to serve as part of the membrane for protonic capacitor formation showed dramatic protonic Al corrosion (*Figure 4*); all the other Al films including the one that was placed in the bulk liquid (P_B) and the one that floated on the anode liquid water surface (P_S) showed no sign of any protonic Al corrosion (*Figures 1, 2, and 3*). Therefore, Silverstein's argument here is clearly invalid or needless.

Silverstein: *(II) Saeed and Lee did not chemically characterize the black material staining the Al films.*

Lee Response: The chemistry of protonic Al corrosion is quite well established in the field. The Saeed and Lee

experiments were focused on experimental demonstration of TELPs. There is no reason to doubt the well-established chemistry of protonic Al corrosion that occurred with excess protons produced by electrolysis of water with platinum electrodes in a pure water-membrane-water system, without the introduction of any other chemicals or corrosive reagents. If you and/or anyone else has any doubt about the protonic (TELPs) Al corrosion on the Al films and wish to "chemically characterize" the protonic Al corrosion staining on the Al films, we would be happy to send samples of the TELPs-corroded Al films for any interested researchers to independently examine.

Silverstein: *(III) All aluminum oxide precipitates, including $Al(OH)_3$, $AlO(OH)$, and Al_2O_3 are white powders. They would not form black stains on the surface of Al film.*

Lee Response: The TELPS-associated Al corrosion stain (gelatinous product precipitate) color often looks dark whitish grey, but it is not "black" as Silverstein claimed. Note that the photographed color of the TELPS-associated Al corrosion gelatinous product precipitate on the Al films could be associated with the corrosion product density, the way the gelatinous product adhered on the Al film surface, and the laboratory lighting conditions. That is, the gelatinous product precipitate color of TELPS-associated Al corrosion on an Al film could vary from light whitish grey to dark (but not "black" as Silverstein claimed) whitish grey, which may represent the differences in the degree (intensity) of TELPS-associated Al corrosion.

Silverstein: *(IV) There is no driving force that would cause aluminum oxide precipitates, all of which are neutral particles, to diffuse toward the Al film. They would simply fall to the bottom of the anode chamber solution or form a colloidal suspension.*

Lee Response: In contrast to Silverstein's claim, the observed dark whitish grey protonic corrosion stain on Al films indicated that the Al^{3+} produced through the TELPS-associated Al corrosion process (Equation 2) could interact with water and be converted to the dark gelatinous whitish grey precipitate of aluminum hydroxide ($Al(OH)_3$) being adhered on site at the Al film surface. Note that the photograph (*Figure 4*) of the live experiment showed that the dark gelatinous whitish grey precipitate of the TELPS-associated Al corrosion stayed on the Al film disk surface; what Silverstein tried to purely speculate that, "They would simply fall to the bottom of the anode chamber solution or form a colloidal suspension" did not occur in our experiments at all. That is, the Al^{3+} produced

through the TELPS-associated Al corrosion did not appear to diffuse far away from the Al surface into the big chamber liquid body since it apparently was soon converted to the gelatinous aluminum hydroxide ($Al(OH)_3$) precipitate at the Al film surface as shown in *Figure 4*.

Silverstein: *(V) Any $Al(OH)_3$ precipitate that did reach the Al film surface would have to diffuse from the relatively alkaline bulk aqueous phase through the acidic surface water layer (pH 2.92). The high proton concentration in the surface layer would dissolve the $Al(OH)_3$ solid particles, giving Al^{3+} (aq) + $3H_2O(l)$.*

Lee Response: Here, Silverstein seems to assume the TELPs as the regular protons that are charge-balanced by their corresponding hydroxyl anions within the same liquid volume so that he could attempt to apply the commonly known water auto-dissociation equilibrium even to the TELPs to calculate the hydroxyl anion concentration in the TELP layer. Unfortunately, his assumption is unlikely to be valid since the corresponding hydroxyl anions for TELPs are the other side of the membrane. That is, TELPs may not be necessarily associated with the water auto-dissociation process that belongs to the bulk liquid phase. Therefore, Silverstein's whole argument here may be questionable (likely to be invalid). In the pure water-membrane-water system, we have experimentally demonstrated that TELPs could not be measured by the bulk liquid phase pH that follows the water auto-dissociation equation ($H_2O = H^+ + HO^-$) but has little to do with TELPs.

Furthermore, for the sake of discussion, even if assuming Silverstein's analysis to be correct (but in fact it is not), Silverstein's argument still could not stand. Note that the thickness of the TELP layer is likely to be only about 1 nm, although its exact thickness is currently not entirely clear. A thickness of 1 nm is a tiny distance in comparison with the micrometer-scale roughness (the microscopic "mountains and valleys") of the Al film surface. Therefore, as TELPs oxidize Al metal atoms and produce Al^{3+} ion and H_2 gas, the so-produced Al^{3+} ion could easily diffuse out of the 1-nm TELP layer and react with hydroxyl anions in nearby liquid water, producing the gelatinous aluminum hydroxide ($Al(OH)_3$) precipitate that can adhere to the microscopic mountains and valleys of the Al film surface. This is still in line with the more or less dark whitish grey gelatinous precipitate that was observed in the photograph of the live experiment (*Figure 4*).

Silverstein: *(VI) Later in their paper (p. 128), Saeed and Lee report that "observable corrosion" forms on the Al film at*

pH > 8.7 in control experiments in the absence of electrolysis. This clearly cannot be from a proton-induced reaction, because at pH > 8.7, the proton concentration is nM or less.

Lee Response: The beaker control experiment with liquid pH > 8.7 was to evaluate the possibility of alkaline (hydroxyl ions) Al corrosion when sodium bicarbonate solution with pH above 8 might be used in the cation-proton exchange experiments. As shown in the Supporting Information (*Figure S2*) of the 2018 Saeed and Lee report (Saeed and Lee, 2018), the alkaline (hydroxyl ions) Al corrosion stain in the Al film looks yellowish, which is qualitatively different from the stain of the protonic Al corrosion that looks more or less dark whitish grey. That is, the hydroxyl anions-based Al corrosion is a completely different process that shall not be confused with the protonic (TELPs) Al corrosion that requires high effective proton concentration with pH < 3.8.

References

Bell WA (1962). Effect of calcium carbonate on corrosion of aluminium in waters containing chloride and copper. Journal of Applied Chemistry 12(2): 53-55. https://doi.org/10.1002/jctb.5010120201

Cherepanov DA, Feniouk, BA, Junge W and Mulkidjanian AY (2003). Low dielectric permittivity of water at the membrane interface: Effect on the energy coupling mechanism in biological membranes. Biophysical Journal 85(2): 1307-1316. https://doi.org/10.1016/S0006-3495(03)74565-2

Dudkina NV, Kouril R, Peters, K, Braun HP and Boekema EJ (2010). Structure and function of mitochondrial supercomplexes. Bba-Bioenergetics 1797(6-7): 664-670. https://doi.org/10.1016/j.bbabio.2009.12.013

Eigen M and De Maeyer L (1958). Self-dissociation and protonic charge transport in water and ice. Proceedings of the Royal Society of London. Series A, Mathematical and Physical Sciences (247): 505-533. https://doi.org/10.1098/rspa.1958.0208

Fuchs EC, Sammer M, Wexler AD, Kuntke P, and Woisetschläger J (2016). A floating water bridge produces water with excess charge. Journal of Physics D: Applied Physics 49(12): 125502. https://doi.org/10.1088/0022-3727/49/12/125502

Fuchs EC, Yntema D, Woisetschläger J (2019). Raman spectroscopy and shadowgraph visualization of excess protons in high-voltage electrolysis of pure water. Journal of Physics D: Applied Physics 52(36): 365302. https://doi.org/10.1088/1361-6463/ab252b

Guan L (2022). Structure and mechanism of membrane transporters. Sci Rep-Uk 12(1): 13248. https://doi.org/10.1038/s41598-022-17524-1

Guffanti A and Krulwich T (1984). Bioenergetic problems of alkalophilic bacteria. Biochem Soc T 12(3): 411. https://doi.org/10.1042/bst0120411

Hariharan P, Bakhtiiari A, Liang R, Guan L (2024). Distinct roles of the major binding residues in the cation-binding pocket of the melibiose transporter MelB. J Biol Chem 300(7): 107427. https://doi.org/10.1016/j.jbc.2024.107427

Heine KB, Parry HA and Hood WR (2023). How does density of the inner mitochondrial membrane influence mitochondrial performance? American Journal of Physiology-Regulatory, Integrative and Comparative Physiology 324(2): R242-R248. https://doi.org/10.1152/ajpregu.00254.2022

Iovine JC, Claypool SM, Alder NN (2021). Mitochondrial compartmentalization: emerging themes in structure and function. Trends Biochem Sci 46(11): 902-917 https://doi.org/10.1016/j.tibs.2021.06.003

Kharel G (2024). Chapter 4: Investigation of calcium and magnesium cation-proton exchange with transmembrane electrostatically localized protons (TELP) at a liquid-membrane interface. In PhD Thesis: Exploring Cation Exchange: Unveiling Its Significance In Biochar And Bioenergetics Applications. Thesis, Old Dominion University, Norfolk, Virginia 23529 USA.

Knyazev DG, Silverstein TP, Brescia S, Maznichenko A, Pohl, P (2023). A New Theory about Interfacial Proton Diffusion Revisited: The Commonly Accepted Laws of Electrostatics and Diffusion Prevail. Biomolecules 13(11): 1641. https://doi.org/10.3390/biom13111641

Krulwich TA, Gilmour R, Hicks DB, Guffanti AA, Ito M (1998). Energetics of alkaliphilic Bacillus species: physiology and molecules. Advances in microbial physiology 40: 401-438. https://doi.org/10.1016/S0065-2911(08)60136-8

Krulwich TA, Liu J, Morino M, Fujisawa M, Ito M, Hicks DB (2011). Adaptive mechanisms of extreme alkaliphiles. Extremophiles handbook, pp. 119-139. https://doi.org/10.1007/978-4-431-53898-1_7

Lapid H, Agmon N, Petersen MK, Voth GA (2004). A bond-order analysis of the mechanism for hydrated proton mobility in liquid water. The Journal of Chemical Physics 122(1). https://doi.org/10.1063/1.1814973

Lee C, Wallace DC, Burke PJ (2024). Super-Resolution Imaging of Voltages in the Interior of Individual, Vital Mitochondria. Acs Nano 18(2): 1345-1356. https://doi.org/10.1021/acsnano.3c02768

Lee JW (2012). Proton-electrostatics hypothesis for localized proton coupling bioenergetics. Bioenergetics 1: 104, 1-8.

Lee JW (2015). Proton-electrostatic localization: explaining the bioenergetic conundrum in alkalophilic bacteria. Bioenergetics 4: 121, 1-8.

Lee JW (2017a). Elucidating the 30-Year-Longstanding Bioenergetic Mystery in Alkalophilic Bacteria. Biophysical Journal 112(3, Supplement 1): 278a-279a. https://doi.org/10.1016/j.bpj.2016.11.1509

Lee JW (2017b). Localized excess protons and methods of making and using the same, PCT International Patent Application Publication No. WO 2017/007762 A1., 56 pages.

Lee JW (2018). Proton motive force computation revealing latent heat utilization by localized protons at a liquid-biomembrane interface. Abstr Pap Am Chem S 255.

Lee JW (2019a). Electrostatically localized proton bioenergetics: better understanding membrane potential. Heliyon 5(7): e01961. https://doi.org/10.1016/j.heliyon.2019.e01961

Lee JW (2019b). Physical Chemistry of Living Systems: Isothermal Utilization of Latent Heat by Electrostatically Localized Protons at Liquid-Membrane Interface. Biophysical Journal 116(3, Supplement 1): 317a. https://doi.org/10.1016/j.bpj.2018.11.1719

Lee JW (2020a). Isothermal Environmental Heat Energy Utilization by Transmembrane Electrostatically Localized Protons at the Liquid-Membrane Interface. Acs Omega 5(28): 17385-17395. https://doi.org/10.1021/acsomega.0c01768

Lee JW (2020b). Protonic Capacitor: Elucidating the biological significance of mitochondrial cristae formation. a Nature research journal: Scientific Reports 10:10304; https://doi.org/10.1038/s41598-020-66203-6 https://doi.org/10.1038/s41598-020-66203-6

Lee JW (2020c). Protonic conductor: better understanding neural resting and action potential. J Neurophysiol 124(4): 1029-1044. https://doi.org/10.1152/jn.00281.2020

Lee JW (2021a). Energy Renewal: Isothermal Utilization of Environmental Heat Energy with Asymmetric Structures. Entropy-Switz 23(6): 665. https://doi.org/10.3390/e23060665

Lee JW (2021b). Mitochondrial energetics with transmembrane electrostatically localized protons: do we have a thermotrophic feature? Sci Rep-Uk 11(1) https://doi.org/10.1038/s41598-021-93853-x

Lee JW (2022a). Type-B Energetic Processes and Their Associated Scientific Implication. Journal of Scientific Exploration 36(3): 487-495. https://doi.org/10.31275/20222517

Lee JW (2022b). Type-B Energy Process: Asymmetric Function-Gated Isothermal Electricity Production. Energies 15(19): 7020. https://doi.org/10.3390/en15197020

Lee JW (2023a). Application of TELC model to neurology:

Review and commentary responding to Silverstein's critique. Current Trends in Neurology 17: 83-89.

Lee JW (2023b). TELP theory: Elucidating the major observations of Rieger et al. 2021 in mitochondria. Mitochondrial Communications 1: 62-72. https://doi.org/10.1016/j.mitoco.2023.09.001

Lee JW (2023c). Thermotrophy Exploratory Study. Journal of Scientific Exploration 37(1): 5-16. https://doi.org/10.31275/20232655

Lee JW (2023d). Transient protonic capacitor: Explaining the bacteriorhodopsin membrane experiment of Heberle et al. 1994. Biophys Chem: 300:107072. https://doi.org/10.1016/j.bpc.2023.107072

Lee JW (2024a). Transient TELC and transmembrane potential in a laser flashed bacteriorhodopsin purple membrane open flat sheet. bioRxiv, 2024.2007.2009.602646. https://doi.org/10.1101/2024.07.09.602646

Lee JW (2024b). Type-B Energetic Processes: Their Identification and Implications. Symmetry 16(7): 808. https://doi.org/10.3390/sym16070808

Markovitch O and Agmon N (2007). Structure and Energetics of the Hydronium Hydration Shells. The Journal of Physical Chemistry A 111(12): 2253-2256. https://doi.org/10.1021/jp068960g

Mitchell P (1985). The Correlation of Chemical and Osmotic Forces in Biochemistry. J Biochem 97(1): 1-18. https://doi.org/10.1093/oxfordjournals.jbchem.a135033

Mitchell P and Moyle J (1967). Chemiosmotic Hypothesis of Oxidative Phosphorylation. Nature 213(5072): 137-139. https://doi.org/10.1038/213137a0

Mulkidjanian AY, Heberle J, Cherepanov DA (2006) Protons @ interfaces: Implications for biological energy conversion. Bba-Bioenergetics 1757(8): 913-930. https://doi.org/10.1016/j.bbabio.2006.02.015

Nicholls DG and Ferguson SJ (2013). Bioenergetics (Fourth Edition). Academic Press, Boston. pp. 53-87 https://doi.org/10.1016/B978-0-12-388425-1.00004-X

Petersen PB and Saykally RJ (2005). Evidence for an Enhanced Hydronium Concentration at the Liquid Water Surface. The Journal of Physical Chemistry B 109(16): 7976-7980. https://doi.org/10.1021/jp044479j

Pourbaix M (1974a). Applications of electrochemistry in corrosion science and in practice. Corros Sci 14(1): 25-82. https://doi.org/10.1016/S0010-938X(74)80006-5

Pourbaix M (1974b). Atlas of electrochemical equilibria in aqueous solutions. National Association of Corrosion, Second Edition. https://doi.org/10.1007/978-1-4684-1806-4_4

Pourbaix, M. 1990. Thermodynamics and corrosion. Corrosion Science 30(10): 963-988. https://doi.org/10.1016/0010-938X(90)90205-J
Rohatgi A (2024). WebPlotDigitizer.

Saeed H (2016). Bioenergetics: Experimental Demonstration of Excess Protons and Related Features. PhD Thesis, Old Dominion University, Norfolk, VA 23529 USA.

Saeed H and Lee J (2018). Experimental determination of proton-cation exchange equilibrium constants at water-membrane interface fundamental to bioenergetics. WATER Journal: 9: 116-140.

Saeed HA and Lee JW (2015). Experimental Demonstration of Localized Excess Protons at a Water-Membrane Interface. Bioenergetics 4: 127, 1-7. https://doi.org/10.1096/fasebj.30.1_supplement.634.1

Santos LP, Ducati TRD, Balestrin LBS, Galembeck F (2011). Water with Excess Electric Charge. The Journal of Physical Chemistry C 115(22): 11226-11232. https://doi.org/10.1021/jp202652q

Scamans GM, Birbilis N, Buchheit RG (2010). Shreir's Corrosion. Editor-in-Chief: Tony, J.A.R. (ed), pp. 1974-2010, Elsevier, Oxford. https://doi.org/10.1016/B978-044452787-5.00095-0

Sheehan DP, Moddel G, Lee JW (2023). More on the demons of thermodynamics. Phys Today 76(3), 13-13. https://doi.org/10.1063/PT.3.5186

Silverstein TP (2023). Lee's transient protonic capacitor cannot explain the surface proton current observed in bacteriorhodopsin purple membranes. Biophys Chem 301:107096. https://doi.org/10.1016/j.bpc.2023.107096

Silverstein TP (2024a). Is localized chemiosmosis necessary in mitochondria? Is Lee's TELP protonic capacitor hypothesis a reasonable model? Mitochondrial Communications 2: 48-57. https://doi.org/10.1016/j.mitoco.2024.06.001

Silverstein TP (2024b). Serious Problems with Saeed & Lee's "Experimental Determination of Proton-Cation Exchange Equilibrium Constants at Water-Membrane Interface Fundamental to Bioenergetics." Water 13: 103-114.

Sukiman N, Hughes A, Thompson G, Mol J, Birbilis N, Garcia S, Zhou X (2012). Durability and corrosion of aluminium and its alloys: overview, property space, techniques and developments, INTECH Open Access Publisher.

Talbot DE and Talbot JD (1998). Corrosion Science and Technology. CRS Press, Boca Raton, Florida. https://doi.org/10.1201/9781420049886

Teixeira P, Galland R, Chevrollier A (2024). Super-resolution microscopies, technological breakthrough to decipher mitochondrial structure and dynamic. Semin Cell Dev Biol 159-160: 38-51. https://doi.org/10.1016/j.semcdb.2024.01.006

Vargel C (2004). Corrosion of aluminium. Elsevier. https://doi.org/10.1016/B978-008044495-6/50012-4

Verdonik DP, Darwin RLD, Williams FW (1999). U.S. Navy Halon 1211 Replacement Program: Assessment of Aircraft Collateral Damage from Dry Chemical Fire Extinguishing Agents, Naval Research Laboratory, Washington, DC.

Zhang C, Knyazev DG, Vereshaga YA, Ippoliti E, Nguyen TH, Carloni P, Pohl P (2012). Water at hydrophobic interfaces delays proton surface-to-bulk transfer and provides a pathway for lateral proton diffusion. P Natl Acad Sci USA 109(25): 9744-9749. https://doi.org/10.1073/pnas.1121227109